# JET FORMATION FROM MASSIVE YOUNG STARS: MAGNETOHYDRODYNAMICS VERSUS RADIATION PRESSURE

Bhargav Vaidya[1], Christian Fendt, Henrik Beuther, and Oliver Porth[1]
Max Planck Institute for Astronomy, Königstuhl 17, D-69117 Heidelberg, Germany; vaidya@mpia.de, fendt@mpia.de

## ABSTRACT

Observations indicate that outflows from massive young stars are more collimated during their early evolution compared to later stages. Our paper investigates various physical processes that impact the outflow dynamics, i.e., its acceleration and collimation. We perform axisymmetric magnetohydrodynamic (MHD) simulations particularly considering the radiation pressure exerted by the star and the disk. We have modified the PLUTO code to include radiative forces in the line-driving approximation. We launch the outflow from the innermost disk region ($r < 50$ AU) by magnetocentrifugal acceleration. In order to disentangle MHD effects from radiative forces, we start the simulation in pure MHD and later switch on the radiation force. We perform a parameter study considering different stellar masses (thus luminosity), magnetic flux, and line-force strength. For our reference simulation—assuming a $30 \, M_\odot$ star—we find substantial de-collimation of 35% due to radiation forces. The opening angle increases from $20°$ to $32°$ for stellar masses from $20 \, M_\odot$ to $60 \, M_\odot$. A small change in the line-force parameter $\alpha$ from 0.60 to 0.55 changes the opening angle by $\sim 8°$. We find that it is mainly the stellar radiation that affects the jet dynamics. Unless the disk extends very close to the star, its force is too small to have much impact. Essentially, our parameter runs with different stellar masses can be understood as a proxy for the time evolution of the star–outflow system. Thus, we have shown that when the stellar mass (thus luminosity) increases with age, the outflows become less collimated.

*Key words:* accretion, accretion disks – ISM: jets and outflows – magnetohydrodynamics (MHD) – methods: numerical – radiative transfer – stars: formation – stars: massive

## 1. INTRODUCTION

Outflows and jets are integral processes of star formation. They are believed to be essential for the angular momentum evolution of the cloud core and the protostar—either directly as stellar winds or indirectly by changing the structure and evolution of the surrounding accretion disk. Outflows from young stars also provide an important feedback mechanism for returning mass and energy into the ambient medium from which the young star is born.

Most of the current understanding about the formation and propagation of jets/outflows comes from observations of low-mass stars. In this case, we are fortunate to know the leading dynamical parameters such as outflow velocity, density, and temperature (e.g., Hartigan & Morse 2007; Ray et al. 2007). In the case of massive young stars many of these parameters are poorly known, although large multi-wavelength studies for massive star-forming regions have been done over the last decade (Beuther et al. 2002a; Stanke et al. 2002; Zhang et al. 2005; López-Sepulcre et al. 2009, 2010; Torrelles et al. 2011). These studies suggest that outflows are an ubiquitous phenomenon not only for low-mass stars, but also in massive star-forming regions. Magnetohydrodynamic (MHD) simulations following the scenario of tower jets along the cloud collapse have also been published, however, only resulting in low velocity out flows (e.g., Banerjee & Pudritz 2006; Machida et al. 2008; Seifried et al. 2011).

The standard framework for the launching process of jets or outflows from low-mass protostars (and most probably also for extragalactic jets) is the model of a disk wind accelerated and collimated by magnetocentrifugal and MHD forces (Blandford & Payne 1982; Pudritz et al. 2007). A number of numerical simulations of jet formation which all confirm this picture of self-collimated MHD jets for low-mass stars have been performed (Ouyed & Pudritz 1997; Krasnopolsky et al. 1999; Fendt & Čemeljić 2002; Ouyed et al. 2003; Fendt 2006, 2009). Its applicability has also been demonstrated for the case of extragalactic jets (e.g., Komissarov et al. 2007; Porth & Fendt 2010).

The formation of the jets around young, still forming high-mass stars takes place in the deeply embedded cold dust and gas cocoons exhibiting large visual extinction of the order of 100–1000 mag (Arce et al. 2007). Recent progress in observations of outflows from young high-mass stars comes from mm and cm wavelengths. Early low-spatial-resolution single-dish studies suggested that massive outflows may have a lower collimation degree than those of their low-mass counterparts (Shepherd & Churchwell 1996). Also, one of the famous outflows, the Orion–KL system, exhibits a more chaotic and not collimated structure (e.g., Schulz et al. 1995). However, later studies indicated that the collimation degree of jets from high-mass protostars can be as high as that from low-mass regions (e.g., Beuther et al. 2002a, 2002b; Gibb et al. 2003; Garay et al. 2003; Brooks et al. 2003; Beuther et al. 2004; Davis et al. 2004). Typical outflow rates in high-mass systems are estimated to be a few times $10^{-5}$ to $10^{-3} \, M_\odot \, \mathrm{yr}^{-1}$, implying accretion rates on the same order of magnitude (e.g., Beuther et al. 2002b).

The originally puzzling result that different studies found different degrees of jet collimation for high-mass star-forming regions could qualitatively be resolved when it was realized that these studies in fact targeted different evolutionary stages. While jets found in the youngest star-forming regions appear similarly collimated as their low-mass counterparts, jets from more evolved (massive) stars exhibit much broader outflow cones.

---

To account for this effect, Beuther & Shepherd (2005) proposed an evolutionary picture for high-mass outflows, where the jet formation starts with similar MHD acceleration processes compared to the low-mass models during the earliest evolutionary stages. However, as soon as the central sources gain significant mass, other processes come into play, for example, the radiation from the central star or more turbulence at the base of the jet. Any combination of this and other processes was expected to lower the degree of collimation. However, the evolutionary sequence proposed by Beuther & Shepherd (2005) was largely observationally motivated and could only provide a qualitative explanation. A thorough theoretical treatment to account for this observational result is still missing—a topic we address in the present paper.

How the radiation field affects the formation of a jet is not obvious a priori. In order to quantify and to disentangle the physical processes involved, a detailed numerical investigation is required. Essentially, stellar (and disk) radiative forces may affect jet acceleration and collimation directly (neglecting ionization, heating, and probably turbulent stirring for simplicity), but also indirectly by changing the physical conditions of the jet launching area, thus governing the mass loading or the initial entropy of the ejected jet material. For example, numerical MHD simulations have shown that jets with higher (turbulent) magnetic diffusivity are expected to be substantially less collimated (Fendt & Čemeljić 2002).

Our previous studies (Vaidya et al. 2009) have shown that the inner accretion disk around massive protostars is ionized, has a high temperature, and is sufficiently gravitationally and thermally stable in order to provide a suitable launching area for an outflow. Together with the recent observations of magnetic fields around high-mass protostars (e.g., Vlemmings 2008; Vlemmings et al. 2010; Girart et al. 2009), this indeed supports the picture of a scaled-up version of low-mass stellar jet formation.

In this paper, we will present a detailed investigation of how a strong radiation field impacts the structure and dynamics of an MHD-driven jet. Motivated by the presence of strong jets and outflows in massive star formation, we apply the standard picture of MHD jet formation known for astrophysical jets and put it in the physical environment of a massive young star.

## 2. MODEL SETUP: JET FORMATION FROM MASSIVE YOUNG STARS

In this section, we discuss the model setup applied for our numerical study concerning the formation of jets and outflows from massive young stars. We are going to consider the main features of the *standard model* of MHD jet formation, which is well established for low-mass young stars, or active galactic nuclei (AGNs) also for high-mass young stars. Our model consists of the following essential ingredients (see Figure 1):

1. A central massive young star that is rapidly evolving in mass $M_*$, luminosity $L_*$, and radius $R_*$.
2. A surrounding accretion disk with a high accretion rate, estimated to be of the order of $\dot{M} \simeq 10^{-3}\ M_\odot\ \mathrm{yr}^{-1}$.
3. A jet launching inner accretion disk. The extension of this area toward the star is not known and may depend on the existence of a strong stellar magnetic field and stellar radiation pressure. Instead of introducing an inner disk radius $R_{\mathrm{in,disk}}$, we will refer to an inner jet launching radius $R_{\mathrm{in,jet}}$, which we presume to be between 0.1 and
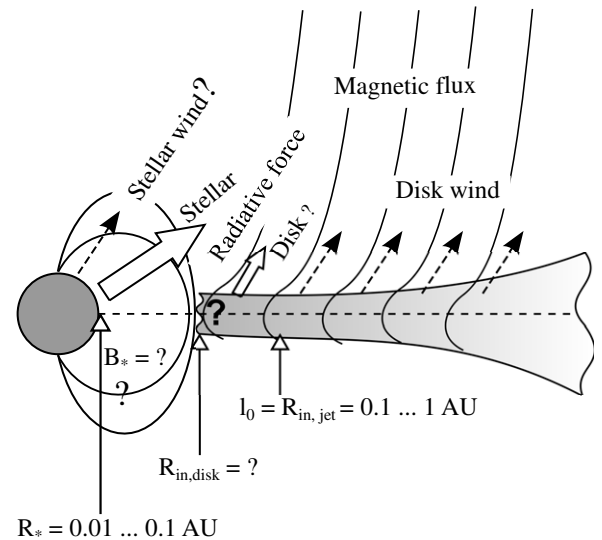


**Figure 1.** Sketch showing our model setup of the inner regions around a massive young star. Several constituents are considered: the disk outflow (dashed arrows) is launched along the magnetic flux surfaces. The innermost launching point is denoted by $R_{\mathrm{in,jet}}$. This outflow is subject to radiation forces (white arrow) from the star and (potentially) from an inner hot accretion disk. The stellar radius $R_*$ could be as large as $\sim 100\ R_\odot$, while the stellar magnetic field structure and strength $B_*$ is rather uncertain. The location of an inner disk radius $R_{\mathrm{in,disk}}$ (if existent) is also not known.

1.0 AU, and to which the length scale of the simulation will be normalized $l_0 = R_{\mathrm{in,jet}}$.
4. A magnetic field around the protostellar object. Magnetic fields are essential for generating collimated high-speed outflows. There exists observational indication for such fields around high-mass protostars.
5. A strong radiation field of the high-mass young star, which may influence accretion and ejection processes. In cases in which the accretion disk reaches down to radii close to the stellar surface (no gap as in the case of low-mass stars), the high disk luminosity may also play a role in the outflow dynamics.

In the following, we briefly discuss the observational and theoretical background of these constituents and finally mention the limits of our model and possible model extensions (a more detailed discussion is provided before the summary).

### 2.1. The Central Massive Young Star

It has been proposed that outflows from massive young stars may follow an evolutionary sequence such that outflows tend to be more collimated and similar to jets from low-mass stars in the early stages of stellar evolution, whereas at later times the outflows are less collimated (Beuther & Shepherd 2005). Since this intrinsically corresponds to an evolutionary sequence in stellar mass, we have investigated simulations with different central masses, ranging from 20 $M_\odot$ to 60 $M_\odot$.

A higher stellar mass automatically gives rise to a faster outflow (supposing the relative launching radius is the same), just because the outflow originates deeper in the gravitational well.

### 2.2. The Accretion Disk and the Jet Launching Area

Jets from low-mass stars are thought to be launched from less than 1 AU of the inner accretion disk (e.g., Anderson et al. 2003; Ray et al. 2007). In T Tauri stars, these regions could be well studied via NIR interferometry (e.g., Akeson et al. 2000,

2005; Dullemond & Monnier 2010). However, to probe regions $\leqslant 100$ AU around a young high-mass star is difficult due to the large degree of extinction. We therefore studied this region via semi-analytic modeling in a previous paper (Vaidya et al. 2009) to understand the physical properties of such disks. We have shown that here the disk may reach high temperatures $\sim 10^5$ K, leading to sublimation of most of the dust and ionizing the bulk of the material.

The inner disk radius in the case of low-mass stars is usually estimated assuming magnetic pressure balanced with the accretion ram pressure. Typical values are $\sim 3$–5 $R_\star$. For young massive stars, such an estimate is not possible due to lack of knowledge of stellar magnetic fields during the formation stage. In addition, radiative force from the bright luminous massive star could influence dynamics of the inner disk. Although our semi-analytic modeling indicated that the disk could extend right down to the central star, detailed three-dimensional models with accurate radiative treatment are required to gain more insight into these close regions.

We have chosen an inner launching point at a distance of $l_0 = 1$ AU from the star (i.e., similar to low-mass stars). A value of $l_0 < 0.1$ AU would imply a high rotation speed and a deep potential well, resulting in a faster outflow. At the same time, the jet launching part of the disk would be much hotter and possibly result in a higher contribution to the radiation force from these hot inner parts. At the other extreme, large jet launching radii $l_0 > 10$ AU will result in slow outflows that are barely affected by stellar and disk radiation forces.

The density $\rho_0$ at the inner launching point is used for physical scaling. We estimate $\rho_0$ from the observed mass fluxes, which are typically of the order of $10^{-3}$–$10^{-5}$ $M_\odot$ yr$^{-1}$, providing $\rho_0 \simeq 10^{-13}$–$10^{-15}$ g cm$^{-3}$ (Section 5.3).

### 2.3. The Magnetic Field

For many years the role of magnetic fields in massive star formation was not really known. However, recent observations have detected relatively strong magnetic fields in massive star-forming regions (Vlemmings 2008). Polarimetric observations of the hot massive molecular core HMC G31.41 have revealed a large-scale hourglass-shaped magnetic field configuration (Girart et al. 2009). Beuther et al. (2010) detected a magnetic field aligned with the molecular outflow via polarimetric CO emission. Further observations have detected synchrotron emission from the proto-stellar jet HH 80-81, indicating a $\sim 0.2$ mG magnetic field in the jet knots while the stellar mass of $\sim 10$ $M_\odot$ is in the range of massive stars (Carrasco-González et al. 2010).

Vlemmings et al. (2010) have measured magnetic field strengths using polarization by 6.7 GHz methanol masers around the massive protostar Cepheus A HW2 and derived a line-of-sight (LOS) magnetic field strength $\sim 23$ mG at a distance of 300–500 AU from the central star. The magnetic field strength is parameterized by the plasma beta, $\beta_0$, which is the ratio of the thermal gas pressure to the magnetic pressure at the inner launching point $l_0$. Our simulations are so far limited to $1 < \beta_0 < 10$ by numerical and physical reasons. This translates into field strengths at 1 AU of $\sim 100$ times weaker than those estimated by conserving magnetic flux using observed values at 300 AU.

Note that it is not only the field strength but also the field *distribution* that affect the jet formation process, as was shown by Fendt (2006) by MHD jet formation considering a wide parameter set of magnetic field and mass flux distribution along the jet launching area. As a result, simulations applying a

**Table 1**
Summary of the Dimensionless Parameters to Study the Impact of
Radiation Forces on the Outflow Dynamics

| Parameter | Definition |
|---|---|
| Eddington ratio (proxy for stellar luminosity) | $\Gamma_e \equiv \frac{\sigma_e L_*}{4\pi c G M_*}$ |
| Luminosity ratio (proxy for disk luminosity) | $\mu \equiv \frac{L_{\rm acc}}{L_*} = \frac{G M_* \dot{M}_{\rm acc}}{R_* L_*}$ |
| Radius ratio (proxy for stellar radius) | $\Lambda \equiv \frac{R_*}{l_0}$ |
| Initial plasma beta (proxy for magnetic field strength) | $\beta_0 \equiv \frac{8\pi P_0}{B_0^2}$ |
| Line-force parameters $Q_0$ and $\alpha$ | Prescribes $M(T)$ using Equation (8) |

concentrated magnetic flux profile tend to be less collimated. We apply as initial field distribution the standard potential field suggested by Ouyed & Pudritz (1997; Section 4.2). A central stellar dipolar field (see Figure 1) is not (yet) supported by observations.

### 2.4. The Stellar and Disk Luminosity

The massive young star produces a substantial luminosity, which is supposed to dynamically change the outflow structure. The dependence of the radiation force on stellar luminosity is parameterized by the Eddington ratio $\Gamma_e$, defined as the ratio of radiation force due to electron scattering to the central gravity (see Table 1). The characteristic values of this dimensionless parameter are obtained from the stellar evolution model of Hosokawa & Omukai (2009). In order to study the impact of radiation forces on the dynamics of outflows, we first launch a collimated jet from a disk wind via MHD forces. Then, after the pure MHD jet has achieved a steady state, we initiate the radiation forces and then compare their impact on the MHD jet. Simulations in which the radiation forces are considered from the beginning (which are computationally much more expensive) end up with a final structure of the outflow similar to the one obtained from the step-by-step method.

We prescribe the radiation force by the line-driving mechanism introduced by Castor, Abbott, & Klein (CAK). Such a force is parameterized by two physical parameters $k$ and $\alpha$. The value of $k$ is proportional to the total number of lines. The quantity $\alpha$ can be considered a measure for the ratio of acceleration from optically thick lines to the total acceleration (Puls et al. 2000). Depending on the selection of lines, for massive OB stars typical values obtained for $k$ range from 0.4–0.6, while $\alpha$ ranges between 0.3 and 0.7 (Abbott 1982). The process of line driving has also been applied to cataclysmic variables (CVs; Feldmeier & Shlosman 1999), as well as to hot and luminous disks around AGNs (Proga et al. 2000; Proga & Kallman 2004).

Proga (2003) carried out numerical simulations of driving winds from hot luminous magnetized accretion disks of AGNs, assuming spherical geometry, an isothermal equation of state, and an initially vertical magnetic field structure. Here we consider a potential field, which is hour-glass shaped, and an adiabatic equation of state.

### 2.5. Limitations of Our Model Setup

Our paper, for the first time, provides a quantitative study of the interplay between radiative and MHD forces on outflows launched from the vicinity of young massive stars, applying

high-resolution axisymmetric numerical simulations. However, a few critical points can be raised which may limit the applicability of our model and which should probably be considered in forthcoming investigations.

From the general point of view there is a lack of true knowledge concerning a number of important parameters, as discussed above. One important question is the location of the inner jet launching radius. If it is identical with an inner disk radius, where is that inner disk radius located, if it exists at all? Is there a strong stellar magnetic field that could open up a gap between the stellar surface and the disk as it is known for low-mass young stars?

Further, our disk model is taken as a boundary condition steady in time. As the star evolves, the disk structure and accretion rate may also evolve in time. This question could only be answered by simulations, solving also for the disk structure. We do not explicitly incorporate heating and cooling but simply consider the adiabatic expansion and compression in the jet.

Another question is the existence of a stellar wind. We know that OB stars have strong mass loss in the form of stellar winds during *later stages* of their lifetimes. The derived mass-loss rates are typically of the order of $10^{-6}$ $M_\odot$ yr$^{-1}$. These winds are primarily radiation driven via the line-driving mechanism (e.g., Kudritzki & Puls 2000; Owocki 2009). The velocities derived are high, ranging from $\sim$500–1000 km s$^{-1}$, and are usually supersonic. However, in the case of high-mass *young* stars, no indication for such winds has been found so far, possibly due to high obscuration. Nevertheless, a future study should implement the physical effect of a central stellar wind.

## 3. BASIC EQUATIONS

For our study, we carry out axisymmetric numerical ideal MHD simulations using the PLUTO code (Mignone et al. 2007). We have modified the original code to incorporate source terms treating the line-driven forces from the central star and disk, consistently taking into account the density and velocity distribution of the outflow.

The MHD code considers the following set of equations, which is the conservation of the mass, momentum, and energy,

$$\frac{\partial \rho}{\partial t} + (\vec{v} \cdot \nabla)\rho + \rho \nabla \cdot \vec{v} = 0, \tag{1}$$

$$\rho \left( \frac{\partial \vec{v}}{\partial t} + (\vec{v} \cdot \nabla)\vec{v} \right) = -\nabla P + \frac{1}{4\pi}(\nabla \times \vec{B}) \times \vec{B} - \rho \nabla \Phi + \rho \vec{F}^{\text{rad}}, \tag{2}$$

$$\frac{\partial}{\partial t}(\rho E) + \nabla \cdot \left[ \rho E \vec{v} + \left( P + \frac{B^2}{8\pi} \right) \vec{v} \right] - \vec{B}(\vec{v} \cdot \vec{B}) = \rho \left[ -\nabla \Phi + \vec{F}^{\text{rad}} \right] \cdot \vec{v}, \tag{3}$$

where $\rho$ is the gas density, $\vec{v}$ is the velocity vector, $P$ is the gas pressure, and $\vec{B}$ is the magnetic field vector with the poloidal and toroidal components $\vec{B}_{\text{p}}$, $B_\phi$. In order to include the radiative forces $\vec{F}^{\text{rad}}$, the relevant source terms have been added in the momentum and energy conservation equation. The total energy density of the flow $E$ comprises contributions from the internal energy $\epsilon$, the mechanical energy, and the magnetic energy,

$$E = \epsilon + \frac{v^2}{2} + \frac{B^2}{8\pi\rho}. \tag{4}$$

The gas pressure in the flow is related to the density assuming an adiabatic equation of state with the adiabatic index $\gamma$,

$$P = (\gamma - 1)\rho\epsilon. \tag{5}$$

The evolution of the magnetic field is governed by the induction equation

$$\frac{\partial \vec{B}}{\partial t} = \nabla \times (\vec{v} \times \vec{B}). \tag{6}$$

We treat the ideal MHD equations without considering resistive terms.

In addition to the above set of equations, the code obeys the condition of divergence-free magnetic fields, $\nabla \cdot \vec{B} = 0$, using the constraint transport method.

### 3.1. Prescription of Radiation Forces

We do not explicitly consider radiative transfer; however, we study the effects of momentum transfer by radiative forces on the outflow matter, which is launched by MHD processes from the underlying disk. The total radiative force $\vec{F}^{\text{rad}}$ is comprised of four contributions—the acceleration due to continuum radiation from the star $\vec{f}_{\text{cont},*}$ and disk $\vec{f}_{\text{cont,disk}}$, respectively, and, similarly, that due to spectral lines from the star $\vec{f}_{\text{line},*}$ and disk $\vec{f}_{\text{line,disk}}$, respectively,

$$\vec{F}^{\text{rad}} = \vec{f}_{\text{cont},*} + \vec{f}_{\text{cont,disk}} + \vec{f}_{\text{line},*} + \vec{f}_{\text{line,disk}}. \tag{7}$$

In the case of young massive stars, the stellar radiation is sub-Eddington. This immediately implies that the continuum force does not contribute to modifying the dynamics of the MHD outflow, as its strength is far below the gravitational pull of the central star. However, line forces could prove to be efficient in substantially enhancing the continuum force by a so-called force multiplier, which is subject to complex theoretical studies of radiative transfer. This theory was first developed by Castor et al. (1975), who solved the radiative transfer equations from spectral lines in moving atmospheres. According to their studies, the force due to line driving can be expressed as a product of force due to continuum radiation and a force multiplier.

The force multiplier depends on two parameters: $k$ and $\alpha$. A "general" parameterization for the force multiplier which is independent of ion thermal velocities $v_{\text{th}}$ (see Equation (A2) in Appendix A) has been introduced by Gayley (1995). In his formulation, the parameter $k$, initially introduced by Castor et al. (1975), has been replaced by a parameter $\bar{Q}$, and the force multiplier can be expressed as follows:

$$M(\mathcal{T}) = k\mathcal{T}^{-\alpha} = \left[ \frac{\bar{Q}^{1-\alpha}}{1-\alpha} \left( \frac{|\hat{n} \cdot \nabla(\hat{n} \cdot \vec{v})|}{\sigma_{\text{e}} c \rho} \right)^\alpha \right], \tag{8}$$

where $\mathcal{T}$ is the optical depth parameter that depends on the LOS velocity gradients (see Equation (A2)). The "strongest form" of this parameterization requires the ansatz $\bar{Q} = Q_0$, where $Q_0$ is the line strength of the strongest line.

Typically for evolved massive stars, the parameter $\bar{Q}$ lies in the range of 1000–2000 (Gayley 1995). For our present study, we have applied the force multiplier considering this "general" parameterization in its "strongest form." Thus, we have the two parameters $Q_0$ and $\alpha$, which define the force multiplier (Equation (8)) and hence the line forces. For simplicity, we assume constant values for these line-force parameters for

a particular simulation run. One of the important properties of the force multiplier $M(\mathcal{T})$ is that its values saturate to a maximum value $M_{\max}$ when the medium becomes optically thin and the optical depth parameter approaches a minimum value, $\mathcal{T} \leqslant \mathcal{T}_{\min}$. The typical value for the maximum force multiplier is relatively constant, $M_{\max} \sim 10^3$, depending only on the metallicity (Gayley 1995).

The line force due to the central star is a product of the force due to continuum from the star and the force multiplier,

$$\vec{f}_{\text{line},*} = \vec{f}_{\text{cont},*} M(\mathcal{T}). \tag{9}$$

The most difficult part of the numerical realization of the line forces is calculating the proper LOS velocity gradients $|\hat{n} \cdot \nabla(\hat{n} \cdot \vec{v})|$ that appears in the formulation of the force multiplier (Equation (8)). Following the definition of this term by Rybicki & Hummer (1978), we express this gradient in terms of the rate-of-strain tensor $e_{ij}$,

$$\hat{n} \cdot \nabla(\hat{n} \cdot \vec{v}) = \sum_{i,j} e_{ij} n_i n_j = \sum_{i,j} \frac{1}{2} \left( \frac{\partial v_i}{\partial r_j} + \frac{\partial v_j}{\partial r_i} \right) n_i n_j, \tag{10}$$

where in general $v_i, r_i,$ and $n_i$ are the components of velocity $\vec{v}$, distance $\vec{r}$, and the unit vector $\hat{n}$, respectively. The different components of this tensor in cylindrical coordinates were calculated from Batchelor (1967). Proga et al. (1998) approximated the above sum to be equal to the most dominant term, corresponding to the radial gradient of flow velocity along the spherical radius. Simulations with a more accurate algorithm including all the other terms to determine the LOS velocity gradient using the above equation have also been carried out (Proga et al. 1999). These simulations show that the qualitative features of winds are not changed as compared to the approximate calculation of the gradients. Further, they are numerically very expensive. We can approximate that the region of consideration is far away from the star, as the central object is a point source. Therefore, the gradient can simply be set as equivalent to $dV_R/dR$, where $R$ is the spherical radius and $V_R$ is the gas velocity along the radius $R$. However, when using cylindrical coordinates instead of spherical coordinates, we have to rewrite Equation (10) by transforming $R$ into $r$, and thereby adding further terms,

$$\hat{n} \cdot \nabla(\hat{n} \cdot \vec{v}) = \frac{1}{1+x^2} \left( \frac{\partial v_r}{\partial r} + x \left( \frac{\partial v_r}{\partial z} + \frac{\partial v_z}{\partial r} \right) + x^2 \frac{\partial v_z}{\partial z} \right), \tag{11}$$

where $x = z/r$.

We have applied two of the line-force components individually as source terms in order to disentangle their effects on the dynamics of a (pure) MHD jet launched from the underlying disk. They are either due to the central star or the underlying hot accretion disk. Disks around massive young stars accrete very rapidly with rates of $10^{-5}\,M_\odot\,\text{yr}^{-1}$ to $10^{-3}\,M_\odot\,\text{yr}^{-1}$. Such high accretion rates imply very high accretion luminosities, in particular in their very inner regions. In order to calculate the line forces due to the disk luminosity, proper geometric factors have to be taken into account. We apply a formulation similar to Pereyra et al. (2000), the details of which are given in Appendix B.

## 4. NUMERICAL SETUP

### 4.1. Grid Setup and Physical Scaling

We perform axisymmetric ideal MHD simulations of jet formation in the presence of radiative forces. Our simulations

are carried out on a grid of physical size $(r \times z) = (52\,l_0 \times 152\,l_0)$, where $l_0$ denotes the physical length scale. The grid is divided into $(512 \times 1024)$ cells in the radial and vertical directions, respectively. Within $r < l_0$ and $z < l_0$ the grid is uniform with a resolution of $\delta r = \delta z = 0.05$, while for $l_0 < r < 50\,l_0$ or $l_0 < z < 150\,l_0$ the grid is stretched with a ratio of 1.002739 and 1.001915 in either the radial or vertical direction, respectively. The remaining outermost part of the grid is again uniform, with cell size $\delta r = 0.125$ and $\delta z = 0.20$, respectively.

Pure MHD simulations would be scale free. However, when radiation is considered, a physical scaling of the dynamical variables becomes essential. Three scaling parameters in physical units are used—the length scale $l_0$, the base flow density $\rho_0$, and the Keplerian velocity $v_0$, at the inner launching point (see Section 2 for physical values used for scaling parameters).

All other quantities can be derived using the following definitions:

$$r_c = \frac{r_{\text{cgs}}}{l_0}, z_c = \frac{z_{\text{cgs}}}{l_0}, \rho_c = \frac{\rho_{\text{cgs}}}{\rho_0}, v_c = \frac{v_{\text{cgs}}}{v_0},$$

$$p_c = \frac{p_{\text{cgs}}}{\rho_0 v_0^2}, B_c = \frac{B_{\text{cgs}}}{B_0} = \frac{B_{\text{cgs}}}{\sqrt{4\pi\rho_0 v_0^2}}. \tag{12}$$

The force multiplier defined in Equation (8) can be expressed in code units as follows:

$$M_c(\mathcal{T}_c) = \left[ \frac{Q_0^{1-\alpha}}{1-\alpha} \left( \frac{v_0}{\sigma_e c \rho_0 l_0 \rho_c} \left| \frac{dv_l}{dl} \right| \right)^\alpha \right]. \tag{13}$$

Quantities with subscript "$c$" are obtained from simulations in the dimensionless form, whereas the quantities with subscript "$cgs$" are the ones required in the physical units. We measure the time $t_c$ in units of $l_0/v_0$. We denote the number of rotations at the inner launching point $l_0$ as $N_{\text{rot}} = l_0/2\pi v_0 = t_c/2\pi$

Using these normalizations the conservation of momentum (Equation (2)) can be written in dimensionless code units,

$$\rho_c \left( \frac{\partial \vec{v}_c}{\partial t_c} + (\vec{v}_c \cdot \nabla_c)\vec{v}_c \right) = \frac{2}{\beta_0}((\nabla_c \times \vec{B}_c) \times \vec{B}_c)$$
$$- \nabla_c P_c - \rho_c \nabla_c \Phi_c + \rho_c (\vec{F}_c^{\text{rad}}), \tag{14}$$

where the plasma beta, $\beta_0 = (8\pi\rho_0 v_0^2)/B_0^2$, specifies the initial strength of the (poloidal) magnetic field at $l_0$ and the radiation force

$$\vec{F}_c^{\text{rad}} = \frac{\vec{F}_{\text{cgs}}^{\text{rad}}}{v_0^2/l_0}. \tag{15}$$

Figure 2 displays the numerical setup used for our simulations. We also show the dynamically important forces that a fluid parcel experiences in an outflow from a young massive star—the gravitational force $\vec{F}_{\text{gravity}}$ by the central star, the Lorentz force components parallel to $\vec{F}_{\text{Lorentz},\parallel}$ (accelerating) and perpendicular to $\vec{F}_{\text{Lorentz},\perp}$ (collimating), the thermal pressure gradient $\vec{F}_{\text{pressure}}$, and the centrifugal force $\vec{F}_{\text{centrifugal}}$, which in particular plays a vital role in accelerating the flow from the disk surface. The essential point of this paper is that we also consider radiation forces from the star and the disk ($\vec{F}_{\text{radiation}}$, Equation (7)). We consider the most dominant radiative source terms, which are those due to the line-driving mechanism from the central massive star and the underlying (hot) disk (see Figure 1).
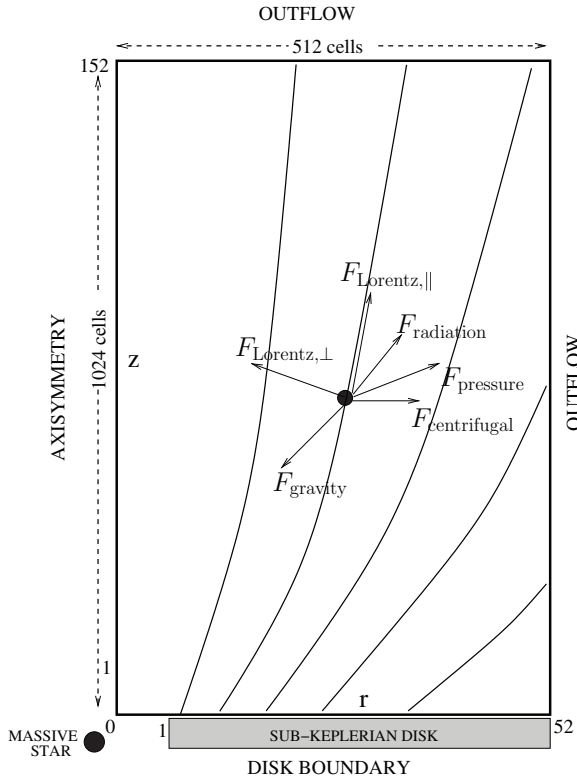
**Figure 2.** Schematic view of the numerical setup along with the definition of the boundary conditions applied for most of the simulation runs. The lines indicate poloidal magnetic field lines anchored in the underlying accretion disk, which is in slightly sub-Keplerian rotation. The dark black spot represents a fluid element frozen onto that field line. Vectors indicate and denote the various forces acting on the fluid element. See the text for a detailed description of the different dynamically important forces.

### 4.2. Initial Conditions

We model the launching of the wind from an accretion disk representing the base of the outflow. The gravitational potential $\Phi$ is that of a point star located at a slight offset $(-r_g, -z_g)$ from the origin to avoid singularity at $r = z = 0$,

$$\Phi(r, z) \propto \left( (r + r_g)^2 + (z + z_g)^2 \right)^{-0.5}, \tag{16}$$

where $r_g = z_g = 0.21$ in all our simulations.

Initially we prescribe a hydrostatic equilibrium with a density distribution

$$\rho(r, z) \propto \left( (r + r_g)^2 + (z + z_g)^2 \right)^{-0.75} \tag{17}$$

(Ouyed & Pudritz 1997). The thermal pressure follows a polytropic equation of state $P = K\rho^\gamma$, with $\gamma = 5/3$. The magnitude of $K = (\gamma - 1)/\gamma$ is determined by the initial hydrostatic balance between gravity and pressure gradients. To begin with, all velocity components are vanishing. Such an initial setup is typical for jet launching simulations (e.g., Ouyed & Pudritz 1997; Krasnopolsky et al. 1999; Fendt 2006). The initial *hot* hydrostatic distribution of density and temperature does not play a significant role in determining the flow structure, as it is eventually washed out by the *cold*, i.e., thermal pressure unimportant, MHD flow that is launched from the base.

The initial magnetic field is purely poloidal (in the $(r, z)$ plane) with a distribution derived from the potential field $\vec{B}_p = \nabla \times A_\phi$ with

$$A_\phi = \frac{\sqrt{r^2 + (z + z_d)^2} - (z_d + z)}{r} \tag{18}$$

(Ouyed & Pudritz 1997), where $z_d$ is considered as the dimensionless disk thickness. Such a magnetic field configuration is force free. Together with the hydrostatic density distribution, this implies an initial setup in force equilibrium. The initial magnetic field strength is prescribed by choice of the plasma-beta $\beta_0$ at the inner launching point.

### 4.3. Boundary Conditions

Choosing the correct physical boundary conditions is of utmost importance for numerical simulations, as they describe the astrophysical system under consideration. In the present setup, we have to deal with four boundary regions (see Figure 2).

#### 4.3.1. Axial Boundary

Along the jet axis, an axisymmetric boundary condition is applied. The normal and the toroidal components of vector fields (i.e., $B_n$, $B_\phi$, $v_n$, $v_\phi$) change sign across the boundary, whereas the axial components are continuous. The density and the pressure are copied into the ghost zones from the domain.

#### 4.3.2. Equatorial Plane Boundary

The "disk boundary" is divided into two regions—the inner gap region extending from the axis to the inner launching radius, $r < l_0$, and further out in the disk region, $r \geqslant l_0$, from which the outflow is launched.

The setup of this boundary is the most crucial for the outflow simulation. This is an "inflow" boundary, with the boundary values determining the inflow of gas and magnetic flux from the disk surface into the outflow. Special care has to be taken to consider the causal interaction between the gas flow in the domain and in the ghost cells.

In order to have a causally consistent boundary condition (Bogovalov 1997; Krasnopolsky et al. 1999; Porth & Fendt 2010), we impose the four physical quantities $\rho$, $\Omega^F$, $P$, and $E_\phi$. The toroidal electric field vanishes, $E_\phi = (\vec{v} \times \vec{B})_\phi = 0$, as result of the ideal MHD approximation. Thus, poloidal velocity and the poloidal magnetic field are parallel at the boundary, $\vec{v}_p || \vec{B}_p$. The angular velocity of the field line (Ferraro's iso-rotation parameter) $\Omega^F$, which is one of the conserved quantities along the field line, is fixed in time along the boundary. We have chosen a Keplerian profile along the disk $\Omega^F(r) \propto r^{-1.5}$. The poloidal velocity at the boundary is "floating," i.e., copied from the first grid cell into the ghost cell each time step. Thus, the mass flux at the disk boundary is not fixed but is consistently derived by the causal interaction between the outflowing gas and the boundary value.

The inner gap region is prescribed as hydrostatic pressure distribution. However, gas pressure gradient, gravity, and centrifugal acceleration are considered for the radial force-balance in the disk, leading to a sub-Keplerian rotation

$$\frac{v_\phi(l_0, 0)}{v_{kep}} = \sqrt{\chi}$$

with $\chi < 1$. Solving for the radial balance delivers the density profile along the boundary

$$\rho_{disk}(r, z) = \left( \frac{1}{1 - \chi} \right) \rho(r, z).$$

Therefore, there is a density contrast between disk and initial corona (the domain). In order to avoid numerical problems at

the interface between the gap and the "inner disk" (i.e., the inner jet launching radius), we smooth this transition using the *Fermi* function, considering

$$\chi = \left( \frac{\chi_0}{1 + \exp(-10(r - 1))} \right).$$

The *Fermi* function is resolved by 16 grid cells. The pressure distribution along the boundary is fixed so as to have a cool disk that is three times denser than the initial corona. Thus, the wind emerging from such a cool disk has a similarly cool temperature (lower than the initial corona). Quantitatively, the average initial coronal temperature within the inner jet launching area is around $5 \times 10^5$ K, while the temperature of the disk surface (i.e., the boundary) in the same area reduces to $5 \times 10^4$ K at 10 AU.

The magnetic field in the boundary is allowed to evolve in time to avoid any current sheets along the interface. When the simulation starts, the rotating disk winds up the poloidal field and induces a toroidal field component. Constraining the field line angular velocity $\Omega^F$ to be constant in time, we need to adjust the rotational velocity of the gas in the boundary,

$$v_\phi = r\Omega^F + \frac{\eta}{\rho} B_\phi, \qquad (19)$$

where the mass load of a field line $\eta = (\rho v_p)/B_p$ is again a conserved quantity in stationary MHD.

### *4.3.3. Outflow Boundaries*

The right and top boundaries (see Figure 2) are defined as outflow boundaries. The canonical outflow conditions (zero gradient across the boundary) are imposed on all scalar quantities and vector components, except for the magnetic field. The toroidal magnetic field component $B_\phi$ in the boundary is obtained by requiring the gradient of the total electric current $I$ to vanish, whereas the poloidal field components are estimated by setting the toroidal current density $j_\phi$ to zero (Porth & Fendt 2010). Having this new outflow condition implemented in the standard PLUTO code, we ensure that there is no artificial collimation due to boundary effects.

## 5. PARAMETER SURVEY

### *5.1. Choice of Governing Parameters*

The three main parameters we apply for a comprehensive study are the (1) central stellar mass $M_*$, (2) plasma-beta $\beta_0$, and (3) the line-force parameter $\alpha$ (see Table 1). We also find that the magnitude of the density at the launching base of the flow $\rho_0$, which is a free parameter in our simulations, strongly affects the flow characteristics (see the discussion in Section 5.3).

We have performed a large parameter study with respect to the central star. The stellar mass considered in our model ranges from $20\,M_\odot$ to $60\,M_\odot$. The size and the luminosity of these stars are obtained from the literature stellar evolution models (Hosokawa & Omukai 2009). The dimensionless parameter that controls the luminosity of the central star is $\Gamma_e$ (see Table 1). Its variation with the stellar masses considered in our model is shown in Figure 3. (also see Section 6.1.5)

We carry simulations for three different values of magnetic field strength $\beta_0 = 1.0, 3.0, 5.0$. We fix the density at the base of the flow to the same value as for the simulations for different stellar mass. Thus, for a $30\,M_\odot$ star and an inner jet launching radius of 1 AU, the different $\beta_0$ values correspond
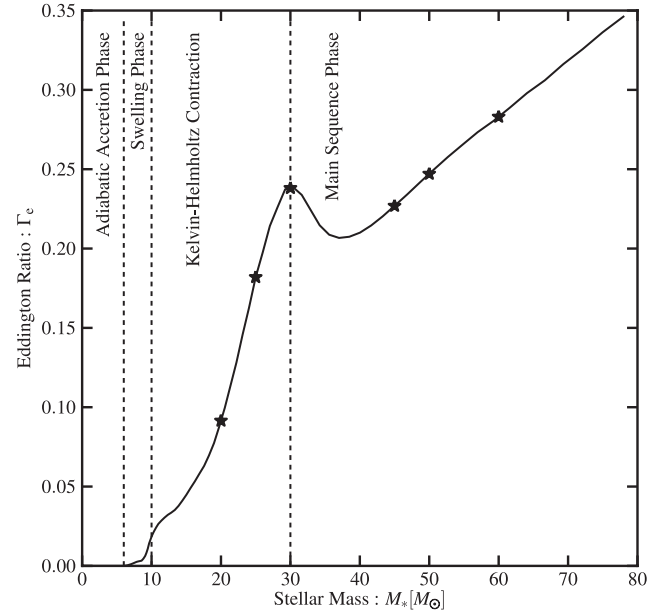


**Figure 3.** Variation of the dimensionless parameter $\Gamma_e$ with stellar mass $M_*$ from Hosokawa & Omukai (2009). The solid black line indicates the stellar mass evolution in the Hosokawa model. Stars represent the Eddington ratio $\Gamma_e$ for different stellar masses in our parameter survey (Section 6.1.5). The vertical dashed lines mark different evolutionary stages for massive young stars accreting rapidly at the rate of $10^{-3}\,M_\odot$ yr$^{-1}$. The curve is obtained using tabulated evolutionary parameters kindly provided by T. Hosokawa (2010, private communication).

to a poloidal magnetic field of 11.5 G, 6.6 G, or 5.1 G at the inner launching point, respectively. Detailed descriptions of the different simulations are shown in Table 2. The jet is launched by pure MHD processes. As it achieves a steady state after, for example, $N_{\rm MHD}$ inner rotations, we switch on the radiative line forces by the central star and run the simulation for another $N_{\rm RAD}$ inner rotations.

The stellar line force in our model is quantified by the parameters $Q_0$ and $\alpha$. In principle, these parameters depend on the degree of ionization in the flow; however, for simplicity, we neglect this dependence and assume that their values remain the same for a particular simulation run. The line force is independent of $Q_0$; however, its dependence on $\alpha$ is strong (Gayley 1995). We fix the line strength parameter $Q_0 = 1400$ for all runs. We carry out simulations with three values of $\alpha = 0.55, 0.60, 0.65$. Although the differences in $\alpha$ seem to be small, they lead to considerable variation in the magnitude of the line forces (Gayley 1995). These values of $\alpha$ and $Q_0$ are consistent with the empirical values obtained for evolved massive stars (Abbott 1982; Gayley 1995). Since, we have no empirical values for these parameters during the formation stage, the present model uses similar values of line-force parameters as obtained from evolved massive stars.

### *5.2. Quantifying the Degree of Collimation*

There are in principal several options for quantifying the collimation degree of jets. Fendt & Čemeljić (2002) suggested comparing the mass fluxes in the radial and vertical directions of the jet as a measure of the jet collimation. However, in general the choice of a "floating" inflow boundary condition and the subsequent time-dependent change of mass fluxes makes it difficult to use them as a measure for the degree of collimation. Therefore, in this work, we quantify the jet collimation by the opening angle $\phi$ of the field lines (which are equivalent

**Table 2**
Parameter Study of Stellar Radiation Line-force Effects on MHD Disk Jets for Different Field Strengths and Stellar Masses

| Run ID | $M_*$ ($M_\odot$) | $\beta_0$ | $\alpha$ | $\phi_A$ | $\phi_F$ | max($\Delta\zeta$[%]) | $\dot{M}_{vert}$ ($M_\odot$ yr$^{-1}$) |
|---|---|---|---|---|---|---|---|
| M30a055b1 | 30 | 1.0 | 0.55 | 21.98 | 16.45 | 5.0 | $3.1 \times 10^{-5}$ |
| M30a055b3 | 30 | 3.0 | 0.55 | 25.63 | 20.68 | 17.0 | $2.9 \times 10^{-5}$ |
| M30a055b5 | 30 | 5.0 | 0.55 | 26.05 | 23.40 | 34.5 | $2.5 \times 10^{-5}$ |
| M30a055b5-c | 30 | 5.0 | 0.55 | 25.55 | 23.01 | 33.9 | $2.4 \times 10^{-5}$ |
| M20a055b5 | 20 | 5.0 | 0.55 | 20.44 | 15.57 | 5.8 | $1.6 \times 10^{-5}$ |
| M25a055b5 | 25 | 5.0 | 0.55 | 23.27 | 19.94 | 21.9 | $2.4 \times 10^{-5}$ |
| M45a055b5 | 45 | 5.0 | 0.55 | 26.84 | 24.35 | 37.7 | $3.0 \times 10^{-5}$ |
| M50a055b5 | 50 | 5.0 | 0.55 | 28.86 | 26.03 | 42.0 | $3.3 \times 10^{-5}$ |
| M60a055b5 | 60 | 5.0 | 0.55 | 31.45 | 29.25 | 56.0 | $3.7 \times 10^{-5}$ |
| M60a060b5 | 60 | 5.0 | 0.60 | 23.73 | 21.48 | 28.7 | $3.2 \times 10^{-5}$ |
| M60a065b5 | 60 | 5.0 | 0.65 | 20.93 | 17.28 | 11.7 | $2.9 \times 10^{-5}$ |
| M25a055b3inj | 25 | 3.0 | 0.55 | 45.84 | 33.87 | 30.2 | $1.3 \times 10^{-5}$ |
| M30a055b3inj | 30 | 3.0 | 0.55 | 47.71 | 36.97 | 37.2 | $1.4 \times 10^{-5}$ |
| M50a055b3inj | 50 | 3.0 | 0.55 | 48.76 | 39.22 | 42.1 | $1.8 \times 10^{-5}$ |

**Notes.** We apply the same physical density at the jet base $\rho_0 = 5.0 \times 10^{-14}$ g cm$^{-3}$, the same inner launching radius $l_0 = 1$ AU, and the same line-force parameter $Q_0 = 1400$ for all runs. The simulations are performed for $N_{MHD} = 319$ inner rotations in the pure MHD, followed by $N_{RAD} = 319$ rotations, with switched-on radiative forces. A measure for the jet opening angle is given at the MHD critical points, $\phi_A$, $\phi_F$, and along the field line rooted at $r = 5.0$ AU. $\Delta\zeta$[%] denotes the percentage difference of the opening angles between the steady-state flows for pure MHD, including radiation force along the field line rooted at the same radius. The vertical mass flux $\dot{M}_{vert}$($M_\odot$ yr$^{-1}$) is measured along the top cells in the domain. The first 10 simulation runs in the table apply a "floating" boundary condition for the injection velocity, while for the last three runs a fixed-mass-flux boundary condition is applied (see Section 6.2).

to velocity streamlines in a steady state). For comparison, we measure the opening angle along a certain field line at two critical points along that field line, the Alfvén point $\phi_A$ and the fast magnetosonic point $\phi_F$. Note that this is not the asymptotic jet opening angle.

In order to estimate the amount of de-collimation $\Delta\zeta$[%] by radiation forces, we measure the angular separation of field lines resulting from $N_{MHD}$ disk rotations from those after $N_{RAD}$ disk rotations,

$$\Delta\zeta[\%](s) = 100\left(\frac{\phi(s, N_{RAD}) - \phi(s, N_{MHD})}{\phi(s, N_{MHD})}\right), \quad (20)$$

where $s$ measures the path along the field line. A positive value of $\Delta\zeta$[%] implies de-collimation, whereas negative values would imply collimation of the jet by radiative forces.

### 5.3. The Outflow Density at the Disk Surface—$\rho_0$

The radiative force term $F_c^{rad}$ is a product of the force multiplier and the continuum force. The force multiplier (Equation (8)) depends on the physical scalings $v_0$, $l_0$, and $\rho_0$ (see Equation (13)). This does imply that each simulation run is unique to the chosen set of scaling parameters for a particular type of star.

In the case of massive stars, these values are currently difficult to measure very close to the star (see Section 2). However, observationally derived values of mass flow rates in molecular outflows and jets around massive stars (Beuther et al. 2002b; Zhang et al. 2005; López-Sepulcre et al. 2009) can be used to constrain the densities with prior assumption of inner jet velocity. Typically measured values of the mass outflow rate are of the order of $10^{-3}$ to $10^{-5}$ $M_\odot$ yr$^{-1}$.

The density $\rho_0$ at the base of the flow ($z \sim 0$) can be estimated by the mass flux launched from the base per unit time,

$$\dot{M}_{out} = 2\pi \rho_0 v_0 l_0^2 \int_{r_{c,min}}^{r_{c,max}} r_c^{1/2-q} dr_c, \quad (21)$$

**Table 3**
Parameter Study of Stellar Radiation Line-force Effects on MHD Disk Jets for Different Jet Density at the Base of the Flow with a Stellar Mass of 30 $M_\odot$

| Runs | $\rho_0$ (g cm$^{-3}$) | $\phi_A$ | $\phi_F$ | max($\Delta\zeta$[%]) | $\dot{M}_{vert}$ ($M_\odot$ yr$^{-1}$) |
|---|---|---|---|---|---|
| M30a055b5d1 | $3.0 \times 10^{-14}$ | 30.30 | 27.79 | 47.7 | $1.5 \times 10^{-5}$ |
| M30a055b5 | $5.0 \times 10^{-14}$ | 26.02 | 23.36 | 34.5 | $2.4 \times 10^{-5}$ |
| M30a055b5d2 | $1.0 \times 10^{-13}$ | 22.91 | 19.47 | 19.6 | $4.3 \times 10^{-5}$ |
| M30a055b5d3 | $5.0 \times 10^{-13}$ | 20.42 | 15.03 | 4.0 | $1.9 \times 10^{-4}$ |

**Note.** For all runs, plasma-$\beta_0 = 5$, $l_0 = 1$ AU and line-force parameters $Q_0 = 1400$ and $\alpha = 0.55$.

where the density at the base of the flow is $\rho(r_c, z_c = 0) = \rho_0 r_c^{-q}$. From Equation (17), q = 3/2. We assume the matter is launched from the disk surface with Keplerian speed (i.e., $v_z(r_c, z_c = 0) = v_0 r_c^{-1/2}$). The physical scalings for the density, velocity, and lengths are $\rho_0$, $v_0$, and $l_0$ respectively, while $r_c$ is the non-dimensional length unit. Thus, the density scaling $\rho_0$ can be expressed as

$$\rho_0 = \frac{\dot{M}_{out}}{2\pi v_0 l_0^2}\left[\ln\left(\frac{r_{c,max}}{r_{c,min}}\right)\right]^{-1}. \quad (22)$$

Using typical observed mass outflow rates for young massive stellar jets, we calculate $\rho_0 \sim 10^{-13}$–$10^{-15}$ g cm$^{-3}$.

The physical value of the density at the base of the flow is in the denominator of Equation (13), and therefore affects the magnitude of the line-driving force significantly. Increasing the density by, for example, a factor of 10, decreases the line force at least by a factor of $10^\alpha$. For the values of $\alpha$ considered here, this magnification could be as large as 3. Such a change in the radiative force clearly has a notable impact on the outflow dynamics, in particular on its degree of collimation. The description of our simulations with different base densities is given in Table 3.
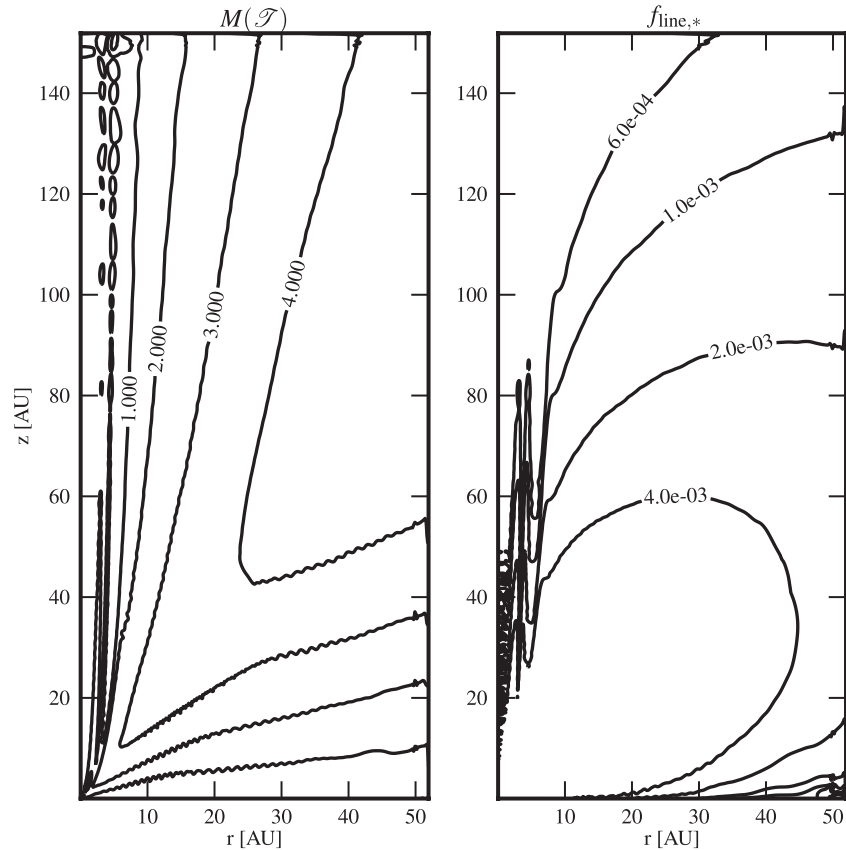
**Figure 4.** Contours of the force multiplier M($\mathcal{T}$) and the specific line radiation force of a central star (in physical units) for the reference simulation M30a055b5 after $N_{\rm rot} = 638$ inner rotations.

## 6. RESULTS AND DISCUSSION

The radiation field in massive star-forming regions may play a crucial role in modifying the dynamics of outflows and jets. In order to disentangle the effects of radiative forces from the pure MHD jet formation, we decided to follow a two-step approach. We first (1) launch a pure MHD disk jet and wait until it reaches a steady state (after about $N_{\rm MHD} = 320$ rotations). We then (2) switch on the radiation line forces and allow the jet flow to further develop into a new dynamic state. In some cases, a new steady-state can be reached, in other cases an unsteady solution develops.

For the radiation forces we consider line forces exerted by (1) the luminous massive young star and by (2) the surrounding accretion disk.

### 6.1. Jet De-Collimation by the Stellar Radiation Field

The radiation line force from the central point star is determined by applying Equation (9). For a detailed physical analysis of the effects of line forces from the star alone, we have chosen simulation M30a055b5 as a reference simulation run (Table 2). The reference run is parameterized for a stellar mass of 30 $M_\odot$, surrounded by an accretion disk with an inner jet launching radius of 1 AU, and a density of $5.0 \times 10^{-14}$ g cm$^{-3}$ at this radius. The initial poloidal magnetic field strength is fixed by a plasma-$\beta_0 = 5.0$. The radiative forces from the star are defined by the line-force parameters $Q_0 = 1400.0$ and $\alpha = 0.55$.

The spatial distributions of the force multiplier $M(\mathcal{T})$ and the specific stellar line force for the reference simulation are both shown in Figure 4. The magnitude of the force multiplier peaks in the top right low-density regions of the flow. This

is expected as the force multiplier increases with decreasing density as shown in Equation (9). In order to calculate the true radiation force, the force multiplier must be convolved with the continuum radiation from the star, resulting in a line-force distribution with a maximum close to the central star (see Figure 4).

The time evolution of the emerging jet[2] is shown in Figure 5, where we display the vertical jet velocity $v_z(r, z)$ and the poloidal magnetic field structure for reference simulation M30a055b5. We clearly see the change from the pure MHD flow (top panels) to the situation when stellar radiation forces are considered (bottom panels).

Material that is injected from the disk surface (bottom boundary) is "frozen" on these field lines (ideal MHD). Initially, the plasma is accelerated magnetocentrifugally and gains substantial speed, producing a bow shock as it propagates. The bow shock leaves the domain after ~60 rotations. Inertial forces of the outflowing mass flux induce a strong toroidal magnetic field component, resulting in magnetic hoop stresses that self-collimate the magnetic field structure together with the hydro-dynamic mass flux. Eventually, when all the dynamical forces along the field line are again balanced, the flow achieves a steady state. The steady-state magnetic field configuration obtained after the pure MHD flow is shown as white dashed lines in Figure 5.

At this stage we "switch on" the line forces of the central star. Immediately, the emergence of a fast axial flow is visible. This flow is unsteady, first forming a knotty structure and then, when

---

[2] Full movies are available for download at
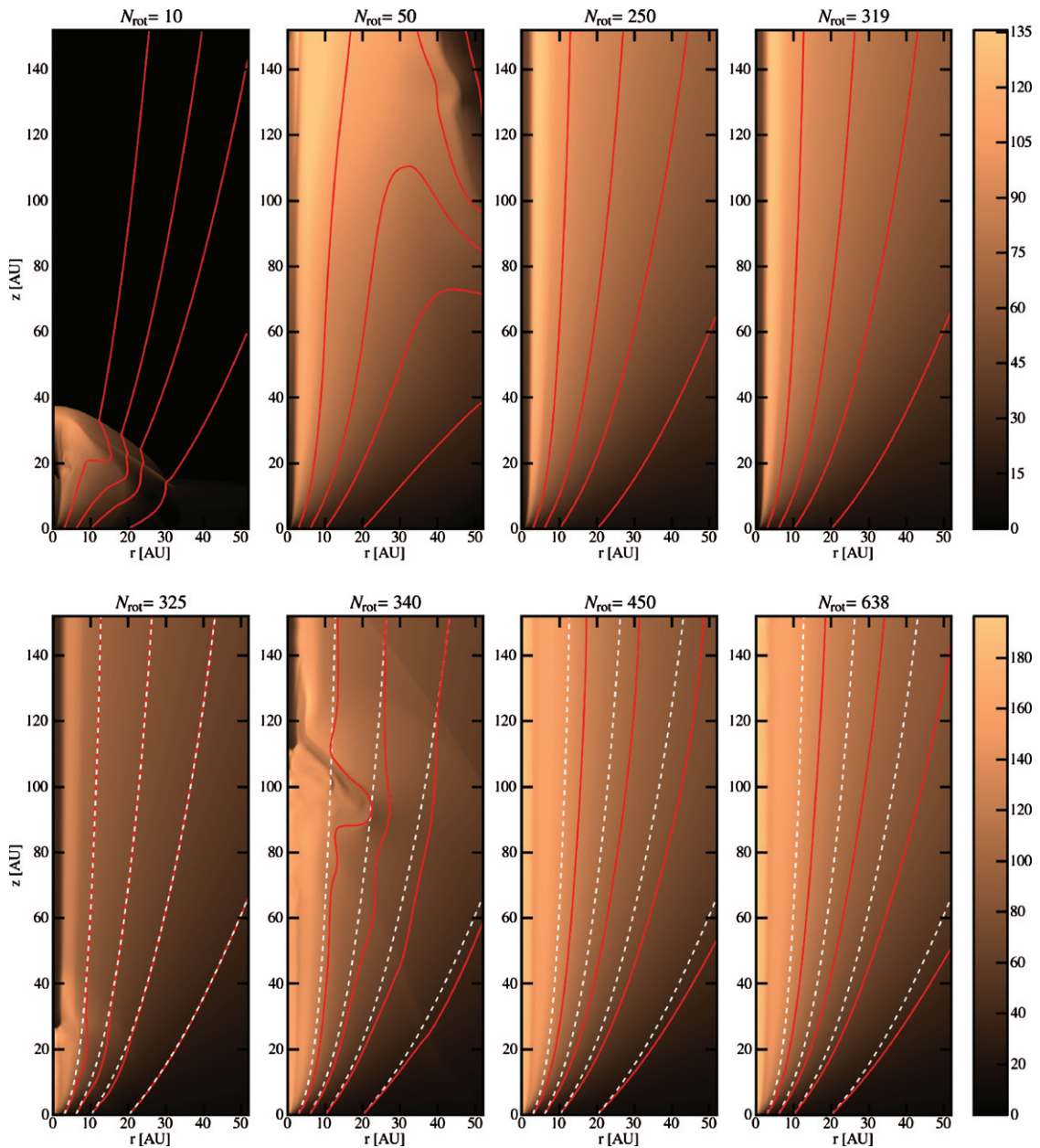http://www.mpia.de/homes/fendt/vaidya/research_bv.html

**Figure 5.** Evolutionary sequence of the reference simulation M30a055b5. Shown are the jet vertical velocity distribution (color coding) and the poloidal magnetic field lines. The color bar represents the velocity scale in km s$^{-1}$ for each row of panels. The series of images are taken at subsequent inner rotations as mentioned on the top of each image. The solid red lines are the poloidal magnetic field lines. To illustrate the impact of radiation forces, we also show the field lines obtained after the steady-state MHD flow for comparison as white dashed lines in the lower four panels.

approaching the upper boundary, stabilizing to a steady axial flow. Jet de-collimation by stellar radiation forces is indicated by the fact that the red solid field lines in the bottom panels of Figure 5 do open up significantly, as compared to field lines in steady-state pure MHD simulation.

When the radiative force is switched on, a shock front begins to propagate into the steady MHD jet (Figure 5). This happens because the additional radiation forces lead to an initial disturbance at the base of the flow, which is then propagated outward. The effect of line forces resulting in a series of propagating shocks is best seen in the poloidal velocity profile along a magnetic field line (see Figure 6). The series of shocks eventually propagates out of the domain, and the flow attains a steady state again. However, the asymptotic outflow velocity that is then achieved is enhanced by a factor of 1.5–2 compared to the pure MHD flow.

We also carry out a run, M30a055b5-c, that includes the radiation force from the beginning along with the MHD flow. This flow evolves into the same configuration as our reference run where the radiation force is later "switched on". This proves that the initial conditions do not affect the final state of the flow. In our study, we prefer to use the step-by-step approach, as it is computationally less expensive.

In summary, we find that radiation forces essentially modify the MHD disk jet in terms of collimation, but also in terms of acceleration and terminal speed.

### 6.1.1. Analysis of the Force-balance in the Outflow

Here we investigate the main forces affecting the outflow dynamics, comparing the magnitudes of various force terms calculated at each grid point along the field line rooted at $r = 5.0$ AU for simulation run M60a055b5. Figure 7 shows such a
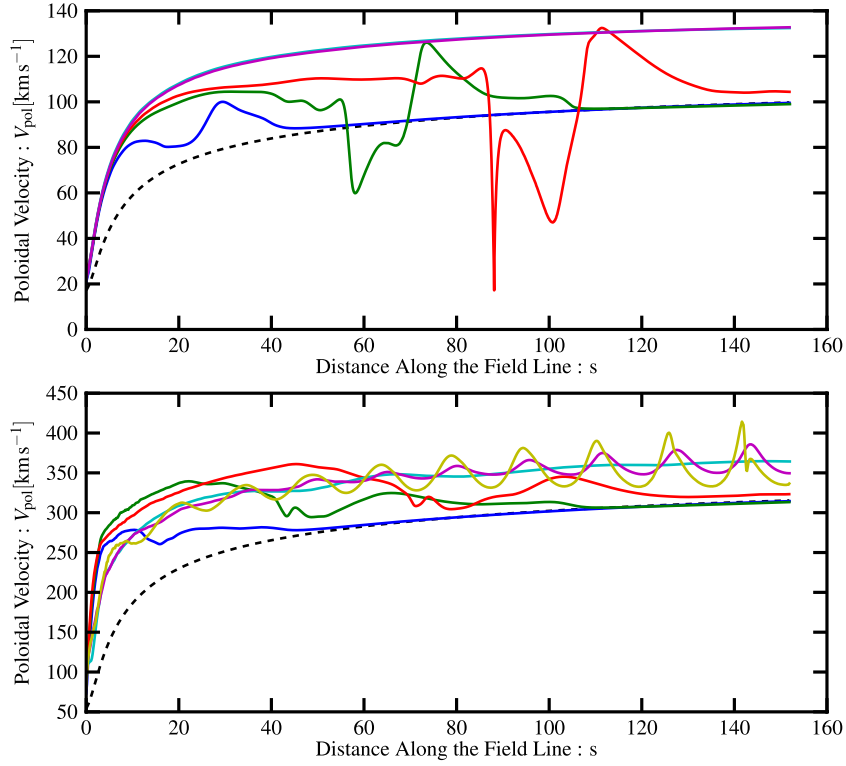
**Figure 6.** Poloidal velocity along the field line rooted at $r = 3$ AU for the two simulations M30a055b5 (top panel) and Disk2 (bottom panel). The distance along the field line $s$ is measured in AU. The various colored solid curves indicate the velocity profile at different inner disk rotations $N_{\rm rot}$ (blue for $N_{\rm rot} = 325$; green for $N_{\rm rot} = 333$; red for $N_{\rm rot} = 340$; cyan for $N_{\rm rot} = 510$; and magenta for $N_{\rm rot} = 638$). The black dotted line in both panels corresponds to the last time step for the pure MHD flow. The solid yellow line shown in the bottom panel indicates the poloidal velocity profile after 1500 inner rotations.
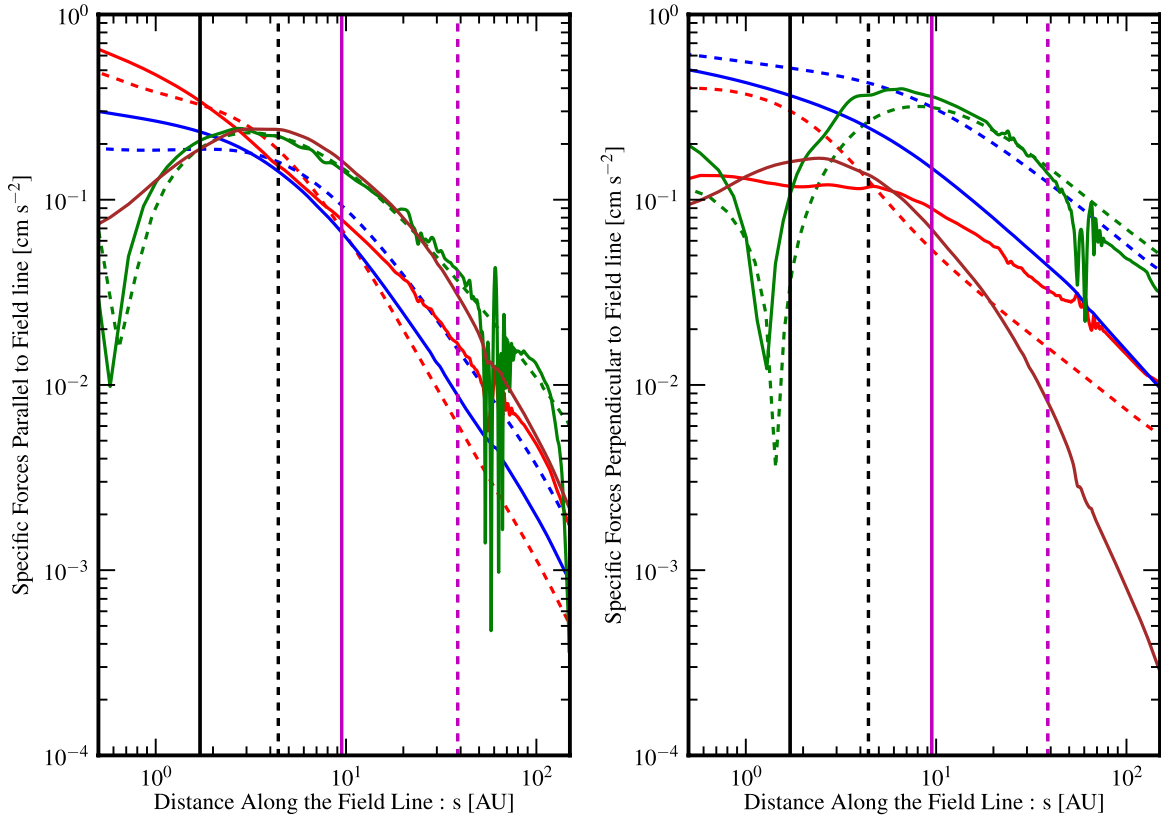


**Figure 7.** Comparison of all specific force terms projected parallel (left) and perpendicular (right) to the field line rooted at $r = 5.0$ AU for the run M60a055b5. Colors specify different specific force terms in dyne cm$^3$ g$^{-1}$—the Lorentz force (green), the gas pressure gradient (red), and the centrifugal force (blue). The dashed lines correspond to the respective force terms for the pure MHD run M60a055b5 (at steady state), while the solid lines represent the forces for the final time step of the simulation including radiative forces. The brown solid line represents the stellar radiation force term for the final time step. The black and magenta vertical solid lines mark the position of the Alfvén and the fast magnetosonic surface for the steady-state flow including radiative forces, whereas the corresponding dashed lines are for the pure MHD flow.
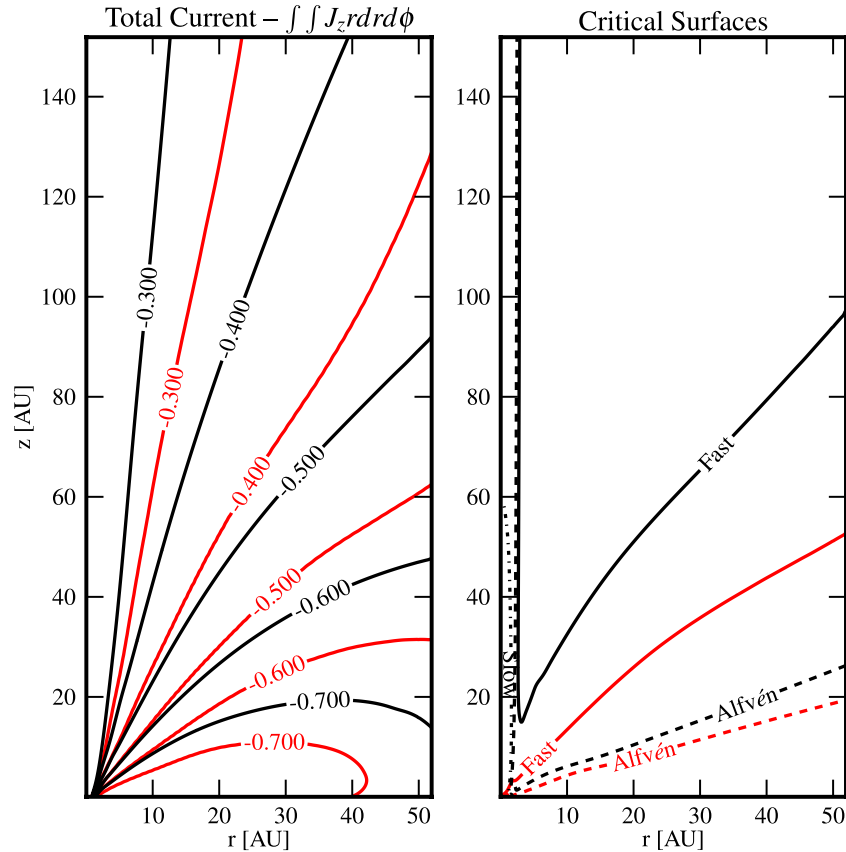
**Figure 8.** Contours of the total poloidal electric current distribution (left) and the location of the MHD critical surfaces (right). In both panels, the pure MHD flow is represented by black solid lines, while the radiative MHD flow is shown with red solid lines.

comparison of specific forces projected *parallel* and *perpendicular* to the field line before and after considering line forces due to stellar radiation. With respect to acceleration, the most striking feature is the enhanced specific pressure gradient force. When radiative forces are considered, the steady MHD flow material at higher altitudes is adiabatically compressed from the underlying accelerated material leading into a shock that propagates out of the domain. The resultant flow has a higher temperature or an increase in thermal pressure. We also find that the gradient of the thermal pressure higher in the flow may increase substantially, such that thermal pressure force and Lorentz force may become comparable. In terms of collimation, it is evident from Figure 7 that the profile of the perpendicular component of the pressure gradient force along the field line becomes flatter than in the case of pure MHD flow. Thus, the pressure force, which was not important for pure MHD flows, now becomes a significant factor in governing the dynamics of the initial flow acceleration (disk wind).

On the contrary, when the line-driving force is switched on in the MHD jet, the centrifugal force becomes reduced by an order of magnitude, particularly at high altitudes in the flow. In order to comprehend this variation of centrifugal force, it is useful to compare the conserved quantities of MHD, in particular the angular velocity of the field line $\Omega_F$. In the pure MHD simulation $\Omega_F$ is conserved throughout the simulation. This also remains true with radiative forces included, simply because $\Omega_F$ is fixed as a boundary value (see Section 4.3). Therefore, the azimuthal velocity at the base of the flow is given by Equation (19). At the same time, the additional line forces accelerate the flow (close to the base) to higher poloidal velocities. The magnetic flux

at the base is fixed as a boundary condition. Hence, the ratio of mass load to density $\eta/\rho$ in Equation (19) increases, and since the toroidal magnetic field $B_\phi$ is negative, the azimuthal velocity decreases. This eventually leads to a decrease of the specific centrifugal force when line forces are considered. The decrease in centrifugal force further implies that the outflow rotates more slowly and that the acceleration close to the base is not only controlled by magnetocentrifugal forces, but also by the thermal pressure force and the radiation force (see Figure 7).

Close to the base of the flow, Lorentz forces are dynamically not important. However, they peak at the Alfvén point of that particular field line. Beyond the Alfvén point, the Lorentz force becomes important and competes with other forces to govern the dynamics of the flow. When radiative force is considered, the Lorentz forces close to the base of the flow and at higher altitudes do not show significant deviations from their values in the pure MHD case.

Line-driven radiative forces have a considerable impact on the poloidal electric current distribution as well as on the critical MHD surfaces in the jet. The contour plots shown in Figure 8 compare the total poloidal current $I = rB_\phi = \int \vec{j}_p d\vec{A}$ and position of critical surfaces before and after considering line-driven forces in the reference simulation M30a055b5. The figure shows that by adding radiative forces (stellar luminosity), the corresponding poloidal electric current density contours are shifted closer to the base of the flow, implying a lower toroidal field strength $B_\phi$ in these jets. We understand this result as a consequence of the lack of jet rotation and thus less effective induction of toroidal magnetic field.

Jet collimation in the conventional Blandford–Payne picture is caused by magnetic hoop stresses ($-B_\phi^2/r$) of the azimuthal magnetic field. The larger toroidal magnetic pressure gradient aids in de-collimating the outflow. A lower $B_\phi$ would not only weaken the hoop stress but also reduce the magnetic pressure ($\sim B_\phi^2$). The decrease of toroidal magnetic pressure would lead to a lower magnetic pressure gradient force. A balance therefore arises between the hoop stress that collimates the flow and the toroidal pressure gradient that de-collimates it. We observe that the field lines de-collimate to a wider configuration on addition of radiative forces, implying that the decrease of toroidal magnetic field has more impact on the reduction of hoop stresses than reducing the magnetic pressure gradient, thus eventually de-collimating the flow.

Considering radiative forces also results in lowering the location of MHD critical surfaces (e.g., slow magnetosonic, fast magnetosonic, and Alfvén surface; see Figure 8). The pure MHD flow is launched marginally super-slowly and sub-Alfvénic. The flow near the axis is, however, sub-slow, due to the boundary condition of conserving the initial hydrostatic density and pressure distribution in the gap region between axis and disk. The flow speed at the critical points depends on the magnetic flux and mass density in the flow. These quantities remain approximately unaltered when radiative forces are considered; thus, the magnetosonic wave speed remains similar as well. Since the radiative line forces now accelerate the wind further to higher velocities, the critical surfaces shift to lower altitudes in the flow (i.e., close to the base of the flow).

We finally note that radiative forces have both direct and indirect effects on the collimation properties of the flow. The radiation force from the star *directly* affects the flow dynamics at its base and close to the star simply by transfer of momentum (Equation (2)), eventually leading to a flow de-collimation. *Indirectly*, the radiation field also enhances the thermal pressure in the flow (Equation (3)) such that the specific pressure force becomes comparable to the Lorentz force, further de-collimating the flow. The resulting opening angles as measured from our reference run at various critical points along the field lines are listed in Table 2. For M30a055b5, the final state of the jet has a steady mass outflow rate of $2.5 \times 10^{-5}$ $M_\odot$ yr$^{-1}$. The opening angles are 26° and 23° at the Alfvén and fast points, respectively, for the field line, which has a foot point $r = 5$ AU. The maximum percentage separation $\Delta\zeta[\%]$ between the opening angles of this field line in the pure MHD flow and that for the flow with radiative forces is 34.5%. A significantly positive value of $\Delta\zeta[\%]$ indicates flow de-collimation. In the following sections, we describe the effects of various physical parameters that could affect the dynamics of the outflow.

### 6.1.2. Radiation Field and Magnetic Field Strength

Here we discuss the interrelation between radiative forces and a variation of magnetic flux, and their combined effect on outflow collimation. We compare simulation runs M30a055b1, M30a055b3, and M30a055b5, assuming for all the same stellar mass 30 $M_\odot$, an inner jet launching radius of 1 AU, and a density at the base of the flow of $5.0 \times 10^{-14}$ g cm$^{-3}$, while the initial magnetic field strength is parameterized by $\beta_0$ ranging from 5.1 G to 11.5 G.

The (initial) pure MHD runs exhibit characteristic differences. A lower $\beta_0$ provides faster jets that are more collimated, simply because the larger field strength provides larger Lorentz forces to collimate and accelerate the flow more efficiently. A lower field strength implies a lower magnetosonic wave speed, resulting
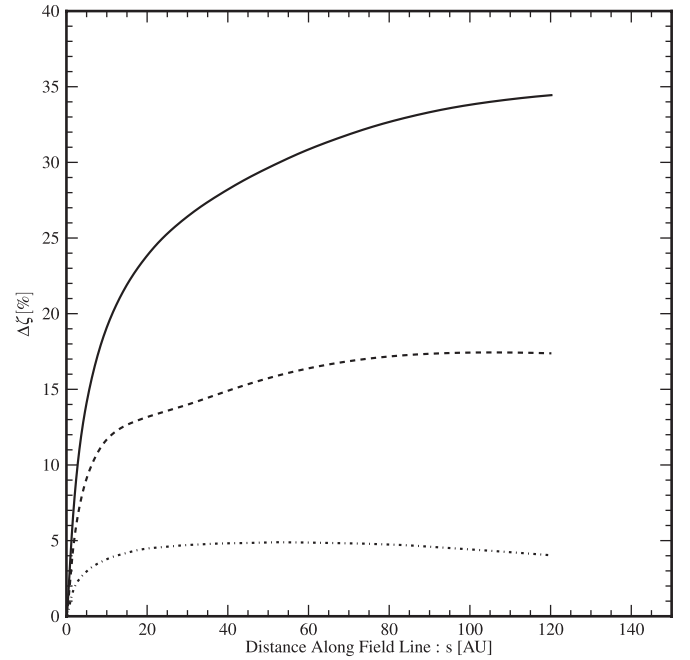


**Figure 9.** Flow collimation along the field line rooted at $r = 5$ AU. Shown is the profile of the percentage separation of field lines between the pure MHD flow and the radiative MHD flow ($\Delta\zeta[\%]$) as a measure of flow collimation. The solid, dashed, and dot-dashed lines are for plasma-$\beta_0 = 5.0, 3.0,$ and $1.0$, respectively.

in magnetosonic surfaces located closer to the disk surface. We cannot simply compare the opening angles at the critical surfaces, as their positions vary in the pure MHD runs with different field strengths. Instead, we quantify the actual *change of opening angle* with and without considering radiative force $\Delta\zeta[\%]$ (i.e., in percentage), as a profile along the field line.

This measure is shown in Figure 9 for a field line rooted at $r = 5$ AU. We see that $\Delta\zeta[\%]$ is significantly positive, indicating that radiative forces do considerably de-collimate the flow. However, the effect of de-collimation is enhanced when the magnetic field strength is reduced (i.e., an increase of $\beta_0$). The asymptotic value of $\Delta\zeta[\%]$ along a field line changes from 35% to 5% when the initial magnetic field strength is increased by a factor of two.

The above analysis for different magnetic field strengths suggests that in the strong field case ($\beta_0 = 1$) jet collimation is controlled by the magnetic forces alone. However, when we decrease the field strength (from 11.5 G to 5.1 G as normalized at 1 AU) the stellar radiation line force begins to compete with the magnetic forces. The resulting jet has a much wider field structure and outflow opening angle, as it is de-collimated as compared to its pure MHD counterpart (see Figure 5). We conclude that radiative forces from the central star (for the chosen parameters) will dominate the magnetic effects in controlling the flow collimation for field strengths $\lesssim 5$ G (at 1 AU). In addition to the field strength the field profile is also important in the dynamical evolution of the jet flow (see Section 2.3). Observational estimates of the field strength in these close regions of massive young stars will further help to narrow the results.

### 6.1.3. Impact of the Line-Force Parameter $\alpha$

The stellar line force is a nonlinear function of $\alpha$. Gayley (1995) showed that a significant change in the mass flux can be obtained with a very slight change in $\alpha$, indicating that this
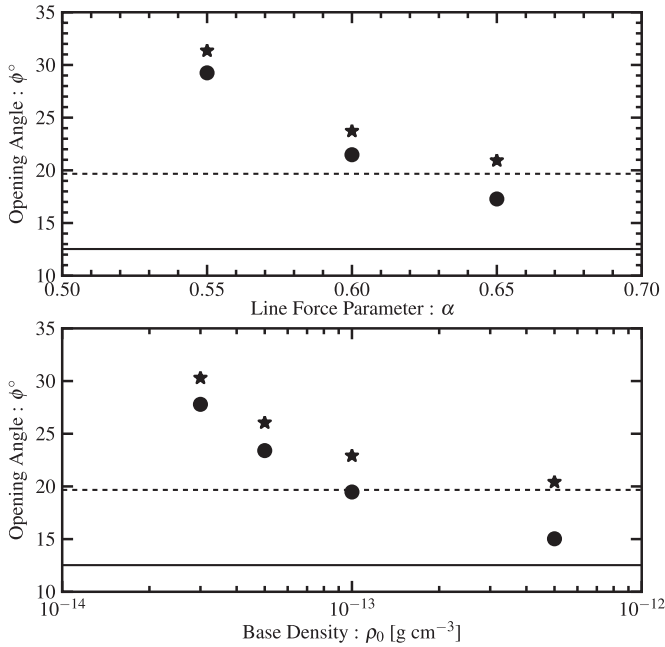
13

**Figure 10.** Jet collimation, jet density, and radiation force. Shown is the opening angle (i.e., the field inclination) at the Alfvén point (stars) and the fast point (dots) of the field line rooted at $r = 5$ AU for runs with different $\alpha$ (top panel) and different jet base density $\rho_0$ (bottom panel). The dotted and solid lines correspond to the opening angle at the Alfvén point, and the fast point of the same field line after the pure MHD flow with an initial plasma-$\beta_0 = 5.0$.

parameter is very sensitive for the calculation of radiative line forces.

Simulation runs M60a055b5, M60a060b5, and M60a065b5 apply the same magnetic field strength ($\beta_0 = 5.0$), but differ in the line-force parameter from $\alpha = 0.55$–$0.65$. A first result is that the increase of $\alpha$ from 0.55 to 0.60 decreases the mass outflow rate significantly by $\sim$16%. We will discuss this interrelation in Section 6.2. However, the outflow opening angles are also affected, as indicated by the top panel of Figure 10. The outflows with lower $\alpha$ become more de-collimated than those with higher $\alpha$.

The above trend indicates that the efficiency of the line-driving mechanism is increased with lower $\alpha$. Physically, a lower $\alpha$ implies a higher contribution of optically thin lines in accelerating the flow. Thus, the dominance of less saturated (i.e., less self-shadowed) lines in accelerating the flow results in an efficient line driving.

In summary, we find that the runs with lower $\alpha$ have higher mass flux and are less collimated. Our results from studying different $\alpha$ are in qualitative agreement with the analytical results from Gayley (1995).

### 6.1.4. Impact of the Density $\rho_0$

In this section, we describe how collimation and acceleration in the outflow are altered with the density at the base of the flow. As mentioned in Section 5.3, the physical mass density applied to scale the numerical simulation is a free parameter in our setup, where we estimate its value from the observations using Equation (22).

Simulation run M30a055b5d1 has the lowest density among all four runs, $\rho_0 = 3 \times 10^{-14}$ g cm$^{-3}$. For this run, the opening angles measured at critical MHD surfaces are larger compared to our reference run. Quantitatively, the opening angles at the Alfvén and the fast surface are $30°$ and $28°$, respectively. Also,
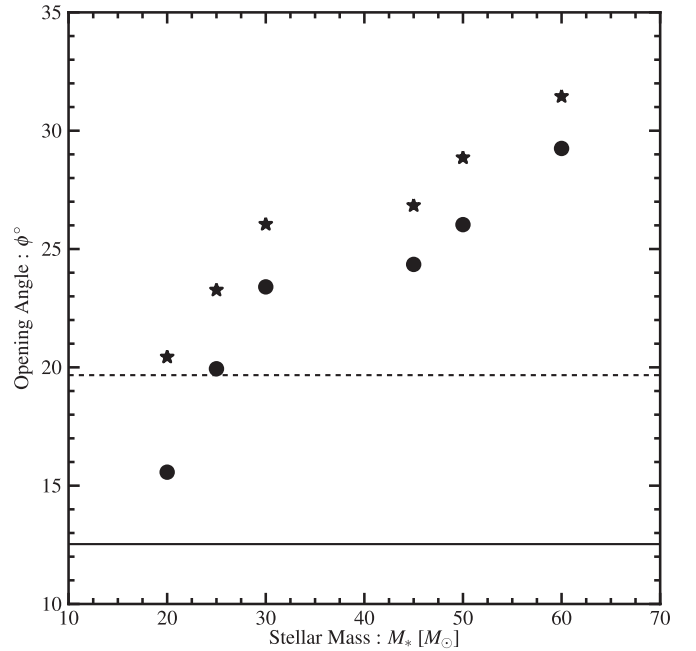


**Figure 11.** Same as Figure 10, but for simulation runs for a different stellar mass.

the maximum percentage change in field line opening angle $\Delta\zeta[\%]$ increases from 35% for the reference run to a staggering high value of 48% for the field line rooted at $r = 5$ AU. In the case of a high jet base density $\rho_0$, the change in the field line opening angle $\Delta\zeta[\%]$ reduces to 4%, with the opening angles at the Alfvén and fast surface being $20°$ and $15°$, respectively (Figure 10).

These results correspond to an inverse correlation of the density at the base of the flow with the force multiplier $M(\mathcal{T})$ (see Equation (13)). Higher densities result in an optically thick environment, thus increasing the optical depth parameter $\mathcal{T}$ and reducing the force multiplier. Thus, the radiative *line-driving* force approaches the limit corresponding to the *continuum* radiation force. Essentially, the continuum force for typical massive young stars is weak compared to other dynamically important forces (for, e.g., gravity).

In summary, we observe the outflow density as one of the leading parameters to govern the dynamics of the outflow by radiation forces. However, observationally this density is very difficult, even impossible, to determine. We thus have to rely on certain assumptions, or may apply estimates of the outflow flux to calculate this density. Our parameter survey considers density values that are consistent with the observed mass fluxes. From our studies, we observe in general that for densities $\rho_0 < 10^{-13}$ g cm$^{-3}$ the line-driving force from the central star is very efficient in accelerating and de-collimating the outflow. However, a denser environment will dilute the influence of the line-driving mechanism.

### 6.1.5. Stellar Mass Evolution and Outflow Collimation

Motivated by the hypothesis of Beuther & Shepherd (2005), we have studied the outflow dynamics and collimation for a sequence of different stellar masses (viz., from 20 $M_\odot$ to 60 $M_\odot$). The change in stellar mass implies a change in the central luminosity. Figure 11 shows the variation of the opening angle at the MHD critical points in simulation runs with central stellar mass. It can be seen that the opening angle varies from $20°$

to 32° for stellar masses from 20 $M_\odot$ to 60 $M_\odot$. The curve rises linearly up to 30 $M_\odot$, but the opening angle does not change considerably with increasing mass.

For the physical parameters of the stellar evolution, such as stellar luminosity and radius, we have applied the *bloating star* model of Hosokawa & Omukai (2009) assuming an accretion rate of $1.0 \times 10^{-3}\,M_\odot\,\mathrm{yr}^{-1}$ (see Figure 3). In this model for massive young stars, the stellar luminosity increases rapidly from 6 $M_\odot$ to 30 $M_\odot$. A star with a high accretion rate undergoes swelling and is considered to bloat up to 100 $R_\odot$. It is the entropy distribution in these stars that causes them to expand that much in size. For stars <10 $M_\odot$, a thin outer layer absorbs most of the entropy from its deep interiors, thereby increasing the entropy in this layer. The rapid increase of entropy in the outer layer of the star causes the star to increase in size (Hosokawa & Omukai 2009). When the stellar mass reaches ∼10 $M_\odot$, the star then begins to shrink (Kelvin–Helmholtz contraction) until its mass reaches ∼30 $M_\odot$. After that, the star approaches the main sequence and then follows the typical main-sequence evolution. The stellar luminosity does not change considerably from $M_* = 30\,M_\odot$ to 40 $M_\odot$—in fact, there is a slight decrease. On the contrary, for stars with mass > 40 $M_\odot$ the stellar luminosity increases with mass. This is reflected as a slight dip in the variation of $\Gamma_e$ with masses of 30 $M_\odot$ and 45 $M_\odot$. Thus, the values of $\Gamma_e$ derived for these two masses do not show considerable difference (0.2381 and 0.2269, respectively). We conclude that the radiation force and hence the dynamics of the outflow do not change to a great extent for these masses.

For simplicity, we keep the inner jet launching radius and the density at the base of the flow fixed for all mass runs. The radiation force is not only altered by changes in $\Gamma_e$, but also due to the physical scaling that appears in the prescription of the force multiplier. In particular, this is the Keplerian velocity at the inner launching radius $l_0$, which is naturally different for different masses and scales with $\sqrt{M_*}$. One would then expect that the radiative force changes by a factor equivalent to $\sqrt{M_*}$. The effect of such a change with increasing central mass not only enhances the mass flux launched from the disk boundary but also imparts to the resulting outflow a wider morphology (see Table 2).

In summary, with the above parameter study of different central stellar masses, we observe that as the luminosity (or mass) of the central star increases, the stellar radiation force becomes relatively stronger. This leads to a higher degree of outflow de-collimation confirming the above-mentioned observational picture of outflow evolution in massive young stars.

### 6.2. Radiation Field and Jet Mass Flux

The simulations presented so far have been performed with "floating" boundary conditions at the base of the flow (see Section 4.3). While these guarantee a causally correct boundary condition ab initio, the disadvantage is that the mass flux emerging from the underlying disk boundary cannot be prescribed a priori. In fact, the mass flux is self-consistently calculated each time step by ensuring continuity of outgoing waves between the domain and the ghost cells. Thus, in our approach applied so far, we fix the initial flow density and float the vertical outflow velocity at the boundary.

The total mass outflow rate ($\dot{M}_{\rm rad} + \dot{M}_{\rm vert}$) in physical units is shown in Figure 12 for runs with different stellar masses and applying a floating boundary condition. The total mass flux has a $\sqrt{M_*}$ dependence for pure MHD runs on converting it
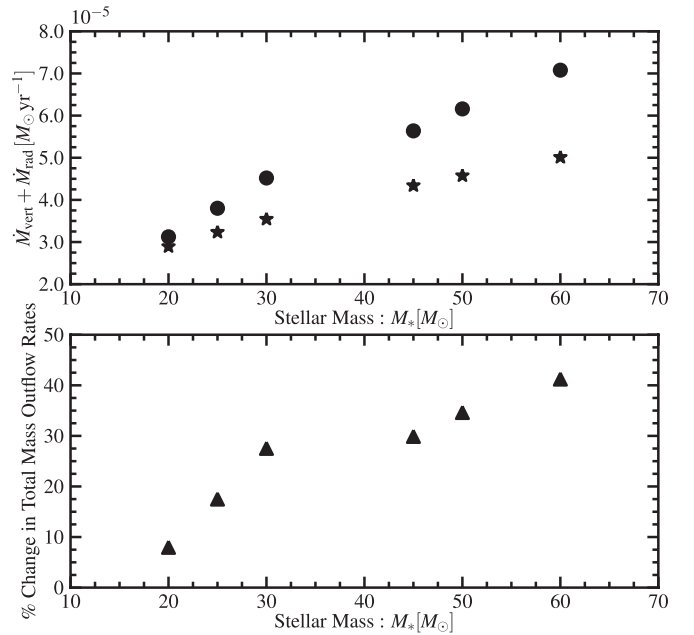


**Figure 12.** Outflow mass flux for simulations applying a different stellar mass. The top panel shows the total mass outflow rates for each star in the case of a pure MHD flow (stars), and for the same outflows including radiative forces (dots). The percentage difference between these mass fluxes is shown in the bottom panel.

to physical units. For a steady-state radiative MHD flow, the physical mass flux also depends on the Eddington parameter $\Gamma_e$, which is related to the stellar luminosity.

The percentage change between these mass outflow rates is shown in the bottom panel of Figure 12. Interestingly, the profile of this curve is similar to the variation of the opening angles (see Figure 11), indicating that the increased mass flux could in fact play a role for de-collimation. Thus, the combination of both the "floating" boundary conditions and the disturbance of the gas physics at the base of the flow by radiative source terms leads to the enhanced mass flux, which modifies the collimation of the flow.

However, the direct effect of radiative force on the flow can also physically deflect the flow and eventually lead to de-collimation. Thus, the problem becomes quite complex as the direct influence of radiative force on the flow is mingled with its second-order effects for, e.g., increase in the mass flux. In order to single out the influence of direct de-collimation effects by radiative forces, we have performed simulations in which we have fixed the outflow mass flux as a boundary condition.

It is essential to inject the outflow with a velocity that is initially supersonic. We fix the mass flux at the boundary by setting the inflow velocity to $v_z = 0.24 \times v_{\rm Kep}$, resulting in a flow with a slow magnetosonic Mach number close to unity and indicating a slightly supersonic flow. In Figure 13 we show the mass outflow flow rates derived along the top ($z = z_{\rm m}$) and right ($r = r_{\rm m}$) boundaries (in red and blue, respectively). We have calculated the radial and vertical mass outflow rates using the following expressions:

$$\dot{M}_{\rm rad} = r_{\rm m} \int_0^{z_{\rm m}} \rho v_r|_{r_{\rm m}} dz, \qquad (23)$$

$$\dot{M}_{\rm vert} = \int_0^{r_m} r \rho v_z|_{z_{\rm m}} dr. \qquad (24)$$
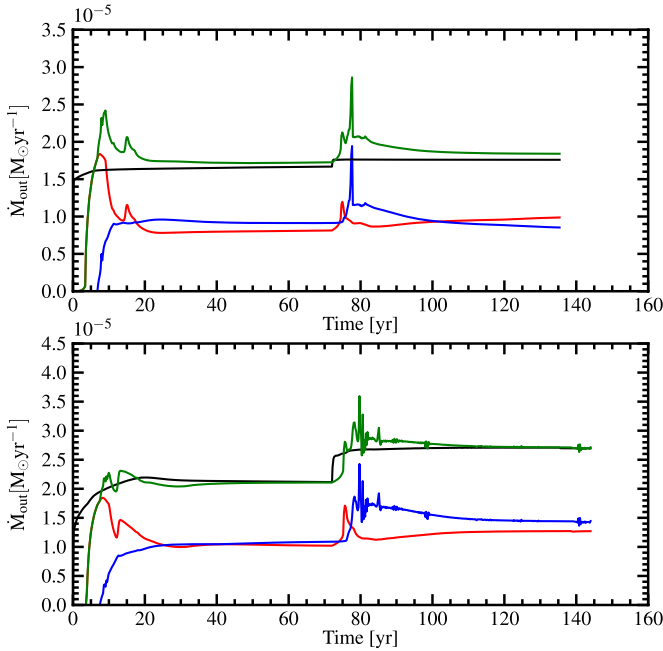
**Figure 13.** Variation of the outflow mass flux with time in simulation runs M30a055b3inj (top panel) and M30a055b5 (bottom panel). The red and blue lines show the variations of the vertical and radial mass fluxes, respectively (see Equations (23) and (24)). The black line corresponds to the mass flux injected from the underlying disk. The green line is the total mass flux leaving the computational domain. Coinciding green and black lines prove conservation of the mass flux.

**Table 4**
Parameter Study of Disk Radiation Line-force Effects on MHD Disk Jets

| Run | $\rho_0$ (g cm$^{-3}$) | max($\Delta\zeta$ [%]) | $\dot{M}_{\rm vert}$ ($M_\odot$ yr$^{-1}$) | Comments |
|---|---|---|---|---|
| Disk1 | $5.0 \times 10^{-14}$ | $-1.8$ | $6.1 \times 10^{-7}$ | Reaches a steady state |
| Disk2 | $5.0 \times 10^{-15}$ | $3.1$ | $7.9 \times 10^{-8}$ | Remains unsteady |

**Notes.** All simulation runs apply the same stellar parameters and line-force parameters as M30a055b5, however, a different inner launching radius of only 0.1 AU. Additionally, two more dimensionless parameters for the disk radiation forces $\mu = 0.4644$ and $\Lambda = 0.4969$ are prescribed (see Table 1).

material away from the axis, resulting in a substantially wider opening angle.

### 6.3. Acceleration by the Disk Radiation Field

We have also carried out a number of simulations that involve only radiation forces caused by a (hot) accretion disk. In principle, in addition to the intrinsic accretion luminosity, the disk radiative force can be enhanced by considering irradiation from the central star (Proga et al. 1998; Drew et al. 1998). For the present model, however, we do not consider irradiation.

Here we present results of two of our simulations, denoted as Disk1 and Disk2 (see Table 4). We have applied the parameter set as for the reference simulation M30a055b5, however, two more parameters governing the dimensionless accretion rate that appears in the accretion luminosity (Equation (B5)) have to be prescribed: the ratio $\mu$ of disk to stellar luminosity, and the ratio $\Lambda$ of stellar radius to inner launching radius (see Table 1). Naturally, a disk extending to radii closer to the center of gravity would have much higher temperatures and thus luminosity (see Vaidya et al. 2009 for an application to massive young stars), and the resulting radiation forces would be able to affect the outflow more.

For the number values applied for these additional parameters we again follow the *bloating star* model (Hosokawa & Omukai 2009), assuming an accretion rate of $10^{-3}$ $M_\odot$ yr$^{-1}$, and an inner jet launching radius of $l_0 = 0.1$ AU and thus obtaining $\mu = 0.4644$ and $\Lambda = 0.4969$. Note that the smaller inner jet launching radius also implies an inner disk radius closer to the star, compared to our models discussed above.

For simulation run Disk2, we have increased the magnitude of the disk radiative force by decreasing the density at the inner jet launching radius by a factor of 10, thus assuming $\rho_0 = 5 \times 10^{-15}$ g cm$^{-3}$. As the radiation force is very sensitive to the density, the lower density at the jet base does increase the radiation force from the disk by a factor of three. Note that, physically, this increase in the disk radiation force could mimic the effects of stellar irradiation.

We quantify the change in collimation degree in runs Disk1 and Disk2 again with the parameter $\Delta\zeta$ [%] (see Equation (20)). Simulation run Disk1 has a maximum of $\Delta\zeta$ [%] $= -1.8$, while run Disk2 has $\Delta\zeta$ [%] $= 3.1\%$. These number values are rather low compared to our simulations with a stellar radiation force indicating that radiation force alone is not strong enough to de-collimate the flow.

Interestingly, simulation run Disk2 shows some unsteady behavior close to the axis, a feature that is absent when only stellar radiation forces are considered. This is consistent with the findings of Proga et al. (1999), who detected a similarly unsteady behavior in their simulations for the case in which the radiative force is dominated by the underlying disk. The fact that we do not see this feature in simulation Disk1 suggests

In the simulations with floating boundary conditions, we observe that the mass flow rate reaches a steady state, first derived self-consistently in the pure MHD flow, and then suddenly increased upon adding the radiative source term. Essentially, this rise is not seen when we apply fixed-mass-flux boundary conditions. However, the fact that the curves of the radial and vertical mass fluxes intersect after $\sim$60 disk rotations after switching on the radiation force is a clear signature of de-collimation. Thus, the modification in terms of collimation due to the *direct* impact of radiative forces on a flow injected with constant mass flux can now be understood with our simulation runs with a priori fixed-mass-flux boundary conditions.

We have thus performed three simulation runs with different stellar masses applying the above-mentioned mass-injection boundary condition (see Table 2). The most evident measure of de-collimation that can be observed is the ratio of vertical to radial mass flow rate. A higher ratio indicates a higher degree of jet collimation. This mass flux ratio for the chosen stellar masses of 25, 30, and 50 $M_\odot$ changes from 1.12 after the steady-state pure MHD flow to 0.92, 0.85, and 0.80 respectively, when radiative force is considered. Note that the radiative forces also accelerate the flow, increasing the maximum velocity for M30a055b3inj in steady-state radiative MHD by a factor of $\sim$1.5 compared to the pure MHD flow.

We also find that de-collimation is mainly due to the *direct* influence of the stellar line-driven force on the outflow, as the amount of mass flux launched into the domain is fixed for these runs (it is thus not a second-order effect resulting from a higher mass flux triggered by the radiation force).

In summary, we conclude here that the line-driving radiation force from the star plays a significant role in directly modifying the dynamics of previously launched MHD flow. This force not only aids in acceleration of the flow, but also pushes the outflow

that the radiative force in run Disk1 is not comparable with the other forces that control the flow dynamics, and that this outflow does correspond more closely to a pure MHD flow. The unsteady flow behavior in run Disk2 is also reflected in the poloidal velocity evolution as steadily propagating "wiggles" in the velocity profile along the field line (or streamline) $v_p(s)$ (Figure 6).

As maximum outflow velocity for the simulations Disk1 and Disk2 we obtain relatively high velocities of $\sim$350 kms$^{-1}$. This is mainly due to the above-mentioned fact that the outflow is launched deeper in the potential well and as close as $l_0 = 0.1$ AU from the central star. Compared to the pure MHD run, we see, however, that the jet that is affected by disk radiation forces only achieves slightly higher asymptotic velocities, as the MHD reaches only $\sim$300 km s$^{-1}$. Thus, the disk radiation force primarily affects the outflow by slightly accelerating it. We do not see any indication that the outflow collimation is affected, which is understandable since the disk radiation force acts mainly in the vertical direction.

In summary, jet acceleration and collimation is rather weakly affected by the disk radiative forces, as their magnitudes are orders of magnitude smaller compared to radiation forces from the central star. However, for other astrophysical jet sources such as CVs and AGNs, the radiative force from the disk could play a significant role. Applying the scaling relations and comparing the amount of energy radiated per unit area from the standard thin disk from a typical young massive star and a standard white dwarf, we obtain from Equation (B1),

$$\frac{D^{\mathrm{MS}}}{D^{\mathrm{WD}}} = 0.06 \left( \frac{10^{-3} \ M_\odot \ \mathrm{yr}^{-1}}{10^{16} \ \mathrm{g \ s}^{-1}} \right) \left( \frac{30 \ M_\odot}{1 \ M_\odot} \right) \left( \frac{0.1 \ \mathrm{AU}}{10^9 \ \mathrm{cm}} \right)^{-3}.$$

(25)

This indicates that the efficiency of line driving due to disk force alone for such massive proto-stellar disks is lower than the compact object accretion disks like CVs, which have been the focus of previous studies by Pereyra & Kallman (2003). This ratio is even smaller if we consider disks around AGNs as considered by Proga & Kallman (2004).

### 6.4. Limitations of Our Model Approach

The main goal of our study was to disentangle the effects of radiative forces from the young star-disk system on a pure MHD outflow launched within the standard picture of magnetocentrifugal, MHD jet formation. In this section, we discuss the limitations of our model approach to the subject of jet formation from massive young stars.

#### 6.4.1. Prescription of Radiation Force

The prescription of radiation force used for the present model does not explicitly consider the radiation transfer. Instead, it implements the radiative force due to lines as a source term in the momentum and the energy equations (see Section 3). This greatly simplifies the numerical task and modeling becomes computationally inexpensive.

#### 6.4.2. Possible Existence of a Stellar Wind

Our model does not consider a stellar wind from the massive young star. Observed outflows around young massive stars are usually thought to have velocities of about 200–500 km s$^{-1}$, a value much smaller than the speed of stellar winds in the evolved stages of OB stars (of about $\sim$1000 km s$^{-1}$). This difference in velocity scale could give a clue to differences in

the environment around the star. During the formation stage, the star is surrounded by dense gas and dust as compared to a more evolved stage where it has cleared all surrounding matter. A rarer environment in a more evolved stage could lead to an efficient acceleration of winds via line driving to 1000 km s$^{-1}$. Hence, for more massive and hotter young stars, impact due to stellar winds could play a vital role in the dynamical evolution of disk winds.

#### 6.4.3. Lack of Knowledge of System Parameters

The inner regions around massive young stars are not accessible with present-day telescopes. Thus, many physical parameters for these inner regions are not observationally constrained (e.g., the inner disk radius, mass density, magnetic field strength). In the present model, we follow the notion that high-mass stars form as scaled-up low-mass stars. Thus, most of the parameters used for the present modeling are derived from estimates for low-mass stars.

#### 6.4.4. Ideal MHD and Line-Force Parameters

Simulations presented here are done using an ideal MHD approximation. This is in principle fine, as ionization fractions are usually high enough to provide good coupling between matter and field. However, for simplicity we have assumed a constant ionization fraction throughout the wind. The radiative force parameters do have explicit dependence on the ionization fraction. The varying temperature across the jet implies varying degree of ionization, which would modify the line-force parameters and thus the value of the force. In this model, we use an idealized assumption of a constant ionization fraction throughout and fix the radiative force parameters for all simulation runs. In the case of non-magnetic CVs, Pereyra & Kallman (2003) have shown that the qualitative effect of the line force is not altered by incorporating local ionization effects for the line-force parameters. However, the importance of such local ionization effects for the case of young massive stars is not known in the literature.

#### 6.4.5. Prescription of the Disk Dynamics

Self-consistent modeling would need to incorporate the time evolution of the disk structure in the simulation and treat the accretion and ejection processes simultaneously. Such simulations are currently performed in general applications of jet launching (e.g., Casse & Keppens 2002; Zanni et al. 2007; Murphy et al. 2010); however, it is too early to be applicable to massive young stars—one reason being the lack of knowledge of the accretion disk parameters (e.g., the question of whether there is a thin or thick disk), another being that radiative effects would have to be implemented in these simulations.

### 7. CONCLUSIONS

We have studied the impact of a line-driven radiation force on the acceleration and collimation of an MHD jet around a young massive stellar object. Our main motivation was to give a solid theoretical understanding of the outflow evolution hypothesis presented by Beuther & Shepherd (2005). For the radiation forces we have considered stellar and disk luminosity. Our basic approach was to initially launch an MHD jet from the underlying disk surface, and then, after the pure MHD outflow had achieved a steady state, to switch on the radiative forces and study their effect on the existing MHD outflow.

We performed a number of simulations with the line-driving force exerted by stellar radiation. These simulations were

performed for a wide range of physical parameters: (1) the central stellar mass, (2) the magnetic flux, and (3) the line-force parameter $\alpha$. In order to apply our method of calculating the line-driving force (CAK approach), we modified the numerical code PLUTO to incorporate appropriate projections of gradients of the two-dimensional velocity field along the light path. Additionally, we consistently implemented these projections for different radiation sources, properly considering the geometry of the radiation field. All these simulations have a "floating" and casually consistent inflow boundary in which the mass flux is not fixed and is derived by the numerical solution.

Our main conclusions from this analysis are as follows.

The line-driven force from the central star for the parameters considered does play a significant role in modifying the dynamics in terms of collimation and acceleration of the outflow. We find that the outflow velocity is increased by a factor of 1.5–2 by radiation forces as compared to the pure MHD flow. Also, the degree of collimation is visibly lowered, e.g., in a 30% change in the magnetic flux profile, or in the wider opening angle of the magnetic field lines.

Investigating different stellar masses, we determine the amount of de-collimation by measuring the opening angles of a typical field line (that with the highest mass flux) at the Alfvén and fast magnetosonic points. We find that for a stellar mass of $20\,M_\odot$, the opening angles are $20°$ and $16°$, respectively. For a $60\,M_\odot$ star these values increase to $32°$ and $29°$, indicating a substantial amount of de-collimation due to the increased stellar luminosity. These findings confirm the observed evolutionary picture for massive outflows, in which more massive stars tend to have outflows of a lower collimation degree. Note that for massive young stars, our results not only constitute a relation of different stellar masses, but also correspond to a time evolution of outflow systems, as the central mass can be substantially increased during massive star formation.

We have also performed simulations with injection of fixed mass flux from the disk boundary for various stellar masses. We find that the ratio of vertical to radial mass flux in these runs decreases from 0.92 to 0.80 with an increase in stellar mass from $25\,M_\odot$ to $50\,M_\odot$. This clearly indicates the fact that the line-driving force from the central star plays an influential role in the physical understanding of the observed evolutionary picture pertaining to outflows from young massive stars.

So far, the magnetic field strength in the jet formation region close to a massive young star-forming region is of an unknown quantity. We therefore have carried out simulations with different field strengths (plasma-$\beta_0 \sim 1.0, 3.0, 5.0$). We find that for the flow with high magnetic flux the radiative forces do not considerably affect the collimation degree. However, for the flow with low magnetic flux, the dynamical effect of radiative forces is greatly increased.

We further find that the line-force parameter $\alpha$ is critical in determining the magnitude of the line-driven forces. Lower values of $\alpha$ lead to an efficient radiative force from the central star and thus de-collimate the flow to a larger extent as compared to higher $\alpha$ values. Since the radiation forces also affect the mass outflow rates for simulations, even a small change in $\alpha$ may lead to significant changes in mass flux of up to $\sim 28\%$.

Line forces due to the hot accretion disk do not play a significant role in controlling the dynamics of the MHD outflow, simply because they are orders of magnitude smaller than all other forces that affect the flow dynamically. Implementing high disk radiation forces has shown that, by taking into account the inner hotter part of the disk, the disk radiation forces will primarily affect the flow acceleration and not the flow collimation.

The source terms for the line-driven forces from the star and the disk implemented in our simulations depend on certain scaling parameters. We find that the physical scaling of the jet density is a leading parameter that affects the flow dynamics. Large densities make it difficult for the line driving to act efficiently, resulting in a flow that is mostly dominated by MHD forces. However, less dense inner regions around massive young stars would allow efficient radiative line driving, and thus accelerate and de-collimate the flow with a great effect.

This paper has addressed the complex problem of jet launching from young massive stars. In doing so, we have applied a simplified prescription of the radiative force rather than a complete radiative transfer calculation. One limitation of our model is the lack of observational knowledge about various parameters particularly very close to the central star. In addition, we have not included effects from stellar winds, which might exist during the *later stages* of young massive star evolution. In spite of these limitations, we find clear evidence of acceleration and de-collimation of jets launched from massive young stars.

In summary, among all the radiative sources considered in studying the dynamics of outflow launched from the young massive star, we see that the line force from the central luminous star is very efficient in de-collimating and accelerating the flow. The line force from the underlying disk is not as significant compared to the stellar force. Also, dynamical effects on the outflow due to the optically thin electron scattering continuum force from the central star and the disk are not significant. Furthermore, we confirm the observed trend of de-collimation seen in outflows from massive stars at different evolutionary stages.

## APPENDIX A

## BASICS OF CASTOR, ABBOTT, AND KLEIN THEORY

According to the CAK theory (Castor et al. 1975), the force multiplier can be expressed as

$$M(\mathcal{T}) = \sum_{\text{lines}} \left( \frac{\Delta \nu_D F_\nu}{F} \frac{1 - e^{-\eta \mathcal{T}}}{\mathcal{T}} \right), \qquad (A1)$$

where $\Delta \nu_D$ is the Doppler shift, $F_\nu$ is the radiation flux at frequency $\nu$, and $F$ is the total integrated flux. The optical depth parameter $\mathcal{T}$ is related to the gradient of velocity, the density in the wind, and the ion thermal velocity $v_{\text{th}}$,

$$\mathcal{T} = \frac{\rho \sigma_e v_{\text{th}}}{|\hat{n} \cdot \nabla(\hat{n} \cdot \vec{v})|}. \qquad (A2)$$

The optical depth parameter $\mathcal{T}$ can be related to the optical depth of a particular line $\tau_L(\hat{n}) = \eta \mathcal{T}$. The *line strength* $\eta$ is the ratio of the line opacity $\kappa_L$ to the electron scattering opacity

$\sigma_e$, while $\hat{n}$ is the unit vector along the LOS. The classification of lines in optically thin and thick lines is done on the basis of interaction probabilities. Optically thick lines are those that have an interaction probability of unity. Lines with optical depths $\tau_L < 1$ are optically thin, and their probability of interaction is $\tau_L$. Based on this approximation, the force multiplier is separable and can be written differently for optical depths that are very high or very low. When the gas is optically thick, $\tau_L > 1$, the force multiplier depends only on the local dynamical quantities of the flow,

$$M_{thick}(\mathcal{T}) = \sum_{thicklines} \left( \frac{\Delta v_D F_\nu}{F} \frac{1}{\mathcal{T}} \right), \qquad (A3)$$

while for the optically thin case $\tau_L < 1$ the force multiplier is independent of the local dynamics, but depends on the line strength of individual thin lines,

$$M_{thin}(\mathcal{T}) = \sum_{thinlines} \left( \frac{\Delta v_D F_\nu}{F} \eta \right). \qquad (A4)$$

In general, for a gas distribution with a mixture of optically thick and thin lines, the empirical form of the total force multiplier integrated over all lines can be expressed as a power law, $M(\mathcal{T}) \sim k\mathcal{T}^{-\alpha}$, where $k$ and $\alpha$ are line-force parameters.

## APPENDIX B

## LINE-DRIVING FORCE DUE TO DISK ALONE

In addition to the line radiative forces from the central star, we also take into account line forces from the underlying disk. The underlying disk cannot be considered as a point source but rather is an extended cylindrical source of radiation. Further, the disk luminosity varies with the radial distance from the central star. In the present simulations, we consider the underlying disk as a steady-state standard thin disk with a temperature profile given by Shakura & Sunyaev (1973). Thus, the energy radiated per unit area $D(r)$ at cylindrical radius $r$ is

$$D(r) = \frac{3\dot{M}_{acc} G M_*}{8\pi r^3} \left[ 1 - \left( \frac{l_0}{r} \right)^{1/2} \right], \qquad (B1)$$

where $\dot{M}_{acc}$ is the steady-state accretion rate onto a central star of mass $M_*$. The inner launching radius is $l_0$. In the case of line forces from the accretion disk, we calculate the radial and vertical radiation flux from the standard disk, $S_r$ and $S_z$, similar to Pereyra et al. (2000). Further, the LOS velocity gradient in the force multiplier applied in the case of disks is for simplicity reduced to $\partial v_z/\partial z$, since the bulk of the radiation flux from the disk is in the vertical direction,

$$\vec{f}_{line,disk} = \frac{\sigma_e}{c} [S_r \vec{r} + S_z \vec{z}] M(\mathcal{T}). \qquad (B2)$$

Here, $S_r$ and $S_z$ are the radial and vertical flux components. Both depend on the disk luminosity and are implemented in the code in their dimensionless forms.

In order to reduce to a dimensionless form, each physical quantity should be written as a product of its value in code units with an appropriate scale factor (see Equation (12)). $S_r$ and $S_z$ are the radial and vertical components of the flux emitted from the disk surface (Hachiya et al. 1998; Pereyra et al. 2000):

$$S_r = \int_0^{2\pi} \int_{l_o}^{end} \frac{D(r')}{\pi}$$
$$\times \frac{z^{\alpha+1}(r - r\cos(\phi))}{[(r^2 + r'^2 + z^2 - 2rr'\cos(\phi))^{1/2}]^{4+\alpha}} r' dr' d\phi, \qquad (B3)$$

$$S_z = \int_0^{2\pi} \int_{l_o}^{end} \frac{D(r')}{\pi}$$
$$\times \frac{z^{\alpha+2}}{[(r^2 + r'^2 + z^2 - 2rr'\cos(\phi))^{1/2}]^{4+\alpha}} r' dr' d\phi, \qquad (B4)$$

where $D(r')$ is the amount of energy radiated per unit area from the standard thin disk (Equation (B1)). In the present simulations, the accretion disk is treated as a boundary and the accretion of matter in the disk is not considered. The mass accretion rate that appears in the above flux radiative components of the disk has to be prescribed on the basis of dimensionless parameters:

$$\dot{M}_{acc} = \frac{4\pi c l_0}{\sigma_e} \Gamma_e \Lambda \mu. \qquad (B5)$$

The radiation flux given above has to be written in dimensionless form to be incorporated into the simulations. The flux components in the code units are given as follows:

$$S_{r,code} = \frac{3cGM_*}{2\pi \sigma_e l_0^2} \Gamma_e \Lambda \mu \int_0^{2\pi} \int_{l_0}^{end} \frac{1}{(r_c')^3} \left( 1 - \sqrt{\frac{1}{r_c'}} \right)$$
$$\times \frac{z_c^{\alpha+1}(r_c - r_c'\cos(\phi))}{[((r_c)^2 + (r_c')^2 + (z_c)^2 - 2r_c r_c'\cos(\phi))^{1/2}]^{4+\alpha}} r_c' dr_c' d\phi, \qquad (B6)$$

$$S_{z,code} = \frac{3cGM_*}{2\pi \sigma_e l_0^2} \Gamma_e \Lambda \mu \int_0^{2\pi} \int_{l_0}^{end} \frac{1}{(r_c')^3} \left( 1 - \sqrt{\frac{1}{r_c'}} \right)$$
$$\times \frac{z_c^{\alpha+2}}{[((r_c)^2 + (r_c')^2 + (z_c)^2 - 2r_c r_c'\cos(\phi))^{1/2}]^{4+\alpha}} r_c' dr_c' d\phi. \qquad (B7)$$

Using the above formulations, the dimensionless radial and vertical components of the line force from the disk can then be obtained. Their respective contours are shown in Figure 14:

$$f_{line,disk}^{r,code}(r_c, z_c) = f_{line,disk}^r / (GM_*/l_0^2) = M_c(\mathcal{T}) S_{r,code}, \quad (B8)$$

$$f_{line,disk}^{z,code}(r_c, z_c) = f_{line,disk}^z / (GM_*/l_0^2) = M_c(\mathcal{T}) S_{z,code}. \quad (B9)$$

The force multiplier for the case of disk force in code units is similar to that used for stellar line force (Equation (13)). However, since we assume that the bulk of the photons from the
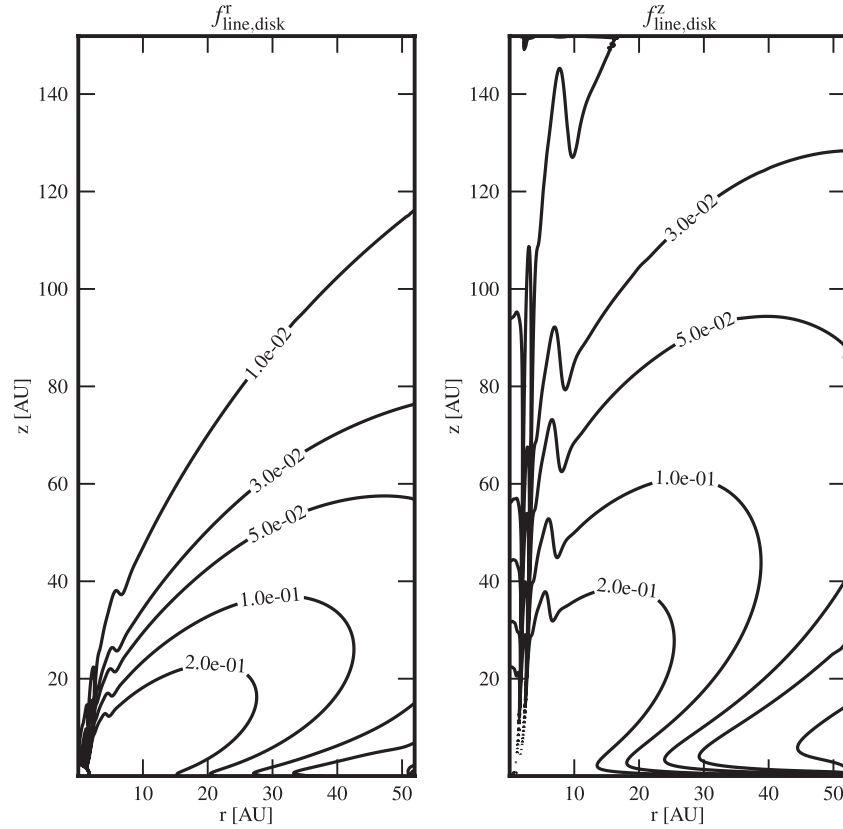
**Figure 14.** Contours of the line force from disk radiation in the radial (left panel) and vertical (right panel) directions. The contour levels are given in physical units. The parameters used are $Q_0 = 1400.0$, $\alpha = 0.55$, $M_* = 30\,M_\odot$, $l_0 = 0.1$ AU, $\rho_0 = 5.0 \times 10^{-14}$ g cm$^{-3}$, $\Gamma_e = 0.2369$, $\Lambda = 0.4969$, $\mu = 0.4644$, and $\beta_0 = 5.0$.

disk move along the vertical $z$-axis, the LOS velocity gradient is approximated to be due only to vertical velocity,

$$\left| \frac{dv_l}{dl} \right| \sim \left| \frac{dv_z}{dz} \right|.$$

The contours of the line force due to the underlying disk in the radial and the vertical direction are shown in Figure 14.

## REFERENCES

Abbott, D. C. 1982, ApJ, 259, 282
Akeson, R. L., Ciardi, D. R., van Belle, G. T., Creech-Eakman, M. J., & Lada, E. A. 2000, ApJ, 543, 313
Akeson, R. L., Walker, C. H., Wood, K., et al. 2005, ApJ, 622, 440
Anderson, J. M., Li, Z.-Y., Krasnopolsky, R., & Blandford, R. D. 2003, ApJ, 590, L107
Arce, H. G., Shepherd, D., Gueth, F., et al. 2007, in Protostars and Planets V, ed. B. Reipurth, D. Jewitt, & K. Keil (Tucson, AZ: Univ. of Arizona Press), 245
Banerjee, R., & Pudritz, R. E. 2006, ApJ, 641, 949
Batchelor, G. 1967, An Introduction to Fluid Mechanics (Cambridge: Cambridge Univ. Press)
Beuther, H., Schilke, P., & Gueth, F. 2004, ApJ, 608, 330
Beuther, H., Schilke, P., Gueth, F., et al. 2002a, A&A, 387, 931
Beuther, H., Schilke, P., Sridharan, T. K., et al. 2002b, A&A, 383, 892
Beuther, H., & Shepherd, D. 2005, in Cores to Clusters: Star Formation with Next Generation Telescopes, ed. M. S. N. Kumar, M. Tafalla, & P. Caselli (New York: Springer), 105
Beuther, H., Vlemmings, W. H. T., Rao, R., & van der Tak, F. F. S. 2010, ApJ, 724, L113
Blandford, R. D., & Payne, D. G. 1982, MNRAS, 199, 883
Bogovalov, S. V. 1997, A&A, 323, 634
Brooks, K. J., Garay, G., Mardones, D., & Bronfman, L. 2003, ApJ, 594, L131
Carrasco-González, C., Rodríguez, L. F., Anglada, G., et al. 2010, Science, 330, 1209

Casse, F., & Keppens, R. 2002, ApJ, 581, 988
Castor, J. I., Abbott, D. C., & Klein, R. I. 1975, ApJ, 195, 157
Davis, C. J., Varricatt, W. P., Todd, S. P., & Ramsay Howat, S. K. 2004, A&A, 425, 981
Drew, J. E., Proga, D., & Stone, J. M. 1998, MNRAS, 296, L6
Dullemond, C. P., & Monnier, J. D. 2010, ARA&A, 48, 205
Feldmeier, A., & Shlosman, I. 1999, ApJ, 526, 344
Fendt, C. 2006, ApJ, 651, 272
Fendt, C. 2009, ApJ, 692, 346
Fendt, C., & Čemeljić, M. 2002, A&A, 395, 1045
Garay, G., Brooks, K. J., Mardones, D., & Norris, R. P. 2003, ApJ, 587, 739
Gayley, K. G. 1995, ApJ, 454, 410
Gibb, A. G., Hoare, M. G., Little, L. T., & Wright, M. C. H. 2003, MNRAS, 339, 1011
Girart, J. M., Beltrán, M. T., Zhang, Q., Rao, R., & Estalella, R. 2009, Science, 324, 1408
Hachiya, M., Tajima, Y., & Fukue, J. 1998, PASJ, 50, 367
Hartigan, P., & Morse, J. 2007, ApJ, 660, 426
Hosokawa, T., & Omukai, K. 2009, ApJ, 691, 823
Komissarov, S. S., Barkov, M. V., Vlahakis, N., & Königl, A. 2007, MNRAS, 380, 51
Krasnopolsky, R., Li, Z., & Blandford, R. 1999, ApJ, 526, 631
Kudritzki, R., & Puls, J. 2000, ARA&A, 38, 613
López-Sepulcre, A., Cesaroni, R., & Walmsley, C. M. 2010, A&A, 517, A66
López-Sepulcre, A., Codella, C., Cesaroni, R., Marcelino, N., & Walmsley, C. M. 2009, A&A, 499, 811
Machida, M. N., Inutsuka, S.-i., & Matsumoto, T. 2008, ApJ, 676, 1088
Mignone, A., Bodo, G., Massaglia, S., et al. 2007, ApJS, 170, 228
Murphy, G. C., Ferreira, J., & Zanni, C. 2010, A&A, 512, A82
Ouyed, R., Clarke, D. A., & Pudritz, R. E. 2003, ApJ, 582, 292
Ouyed, R., & Pudritz, R. E. 1997, ApJ, 482, 712
Owocki, S. 2009, in AIP Conf. Ser. 1171, ed. I. Hubeny et al. (Melville, NY: AIP), 173
Pereyra, N. A., & Kallman, T. R. 2003, ApJ, 582, 984
Pereyra, N. A., Kallman, T. R., & Blondin, J. M. 2000, ApJ, 532, 563
Porth, O., & Fendt, C. 2010, ApJ, 709, 1100
Proga, D. 2003, ApJ, 585, 406

Proga, D., & Kallman, T. R. 2004, ApJ, 616, 688
Proga, D., Stone, J. M., & Drew, J. E. 1998, MNRAS, 295, 595
Proga, D., Stone, J. M., & Drew, J. E. 1999, MNRAS, 310, 476
Proga, D., Stone, J. M., & Kallman, T. R. 2000, ApJ, 543, 686
Pudritz, R. E., Ouyed, R., Fendt, C., & Brandenburg, A. 2007, in Protostars and Planets V, ed. B. Reipurth, D. Jewitt, & K. Keil (Tucson, AZ: Univ. of Arizona Press), 277
Puls, J., Springmann, U., & Lennon, M. 2000, A&AS, 141, 23
Ray, T., Dougados, C., Bacciotti, F., Eislöffel, J., & Chrysostomou, A. 2007, in Protostars and Planets V, ed. B. Reipurth, D. Jewitt, & K. Keil (Tucson, AZ: Univ. of Arizona Press), 231
Rybicki, G. B., & Hummer, D. G. 1978, ApJ, 219, 654
Schulz, A., Henkel, C., Beckmann, U., et al. 1995, A&A, 295, 183

Seifried, D., Pudritz, R. E., Banerjee, R., Duffin, D., & Klessen, R. S. 2011, MNRAS, submitted (arXiv:1109.4379)
Shakura, N. I., & Sunyaev, R. A. 1973, A&A, 24, 337
Shepherd, D. S., & Churchwell, E. 1996, ApJ, 457, 267
Stanke, T., McCaughrean, M. J., & Zinnecker, H. 2002, A&A, 392, 239
Torrelles, J. M., Patel, N. A., Curiel, S., et al. 2011, MNRAS, 410, 627
Vaidya, B., Fendt, C., & Beuther, H. 2009, ApJ, 702, 567
Vlemmings, W. H. T. 2008, A&A, 484, 773
Vlemmings, W. H. T., Surcis, G., Torstensson, K. J. E., & van Langevelde, H. J. 2010, MNRAS, 404, 134
Zanni, C., Ferrari, A., Rosner, R., Bodo, G., & Massaglia, S. 2007, A&A, 469, 811
Zhang, Q., Hunter, T. R., Brand, J., et al. 2005, ApJ, 625, 864